GEOLOGY AND GEOPHYSICS OF THE CIENEGA BASIN AREA, PIMA AND COCHISE COUNTIES, ARIZONA

by

Stephen M. Richard and Raymond C. Harris

Arizona Geological Survey
Open-File Report 96-21

September, 1996

Arizona Geological Survey
416 W. Congress, Suite #100, Tucson, Arizona 85701

Final Report to the Arizona Department of Water Resources
Water Protection Fund Grant 95-016WPF

This report is preliminary and has not been edited
or reviewed for conformity with Arizona Geological Survey standards

CONTENTS

CONTENTS i
LIST OF FIGURES i
LIST OF PLATES ii
LIST OF TABLES ii
GEOLOGIC SETTING OF BASIN 1
MAGNETIC DATA 2
  NURE data 2
  Tombstone survey 2
GRAVITY DATA 3
SAKI 3
PHYSICAL PROPERTIES OF ROCKS 3
  Discussion of Cross sections 4
  Section A-A' 4
  Section B-B' 5
  Section C-C' 14
  Section D-D' 15
EVALUATION OF MODELING PROCEDURE 15
GEOLOGIC SYNTHESIS 18
  Mesozoic structures 18
  Middle Tertiary history 22
COMPARISON WITH PREVIOUS MODEL 23
CONCLUSIONS 23
REFERENCES 24
APPENDIX 1: MODEL DESCRIPTIONS. 25

LIST OF FIGURES

Figure 1. Location of Cienega basin study area.
Figure 2. Explanation of unit abbreviations used on cross sections.
Figure 3. Cross section models and calculated gravity and magnetic anomalies for section A-A'
Figure 4. Geologic cross section A-A'
Figure 5. Cross section models and calculated gravity anomaly for section B-B'
Figure 6. Geologic cross section B-B'
Figure 7. Cross section models and calculated gravity anomaly for section C-C'
Figure 8. Cross section models and calculated magnetic anomaly for section C-C'
Figure 9. Geologic cross section C-C'
Figure 10. Cross section models and calculated gravity and magnetic anomalies for section D-D'
Figure 11. Geologic cross section D-D'
Figure 12. Simplified gravity model for section B-B'

Figure 13. Separation of anomalies due to basin fill units (Tp and QTg) and bedrock units.
Figure 14. Mesozoic structural and stratigraphic features of the Cienega Gap study area. Stippled area is pre-Tertiary bedrock outcrop. Strike and dip data are for Bisbee Group strata. Base map is portion of base map used for Plate 1. Scale 1:100,000 (same as plates).
Figure 15. Features related to middle Tertiary sedimentation and extension. Stippled area is pre-Tertiary bedrock outcrop. Base map is portion of base map used for Plate 1. Scale 1:100,000 (same as plates). Tpl is lower Pantano Formation (Tpl, Tpf, and Tpv on Plate 1), Tpu is upper Pantano formation (Tpm on Plate 1).
Figure 16. Younger basin-fill related sedimentation and structure. Stippled area is pre-Tertiary bedrock outcrop. Base map is portion of base map used for Plate 1. Scale 1:100,000 (same as plates).
Figure 17. Locations of wells from which lithologic data was obtained for this study.

LIST OF PLATES

Plate 1: Geologic map of the lower Cienega Basin area, Pima and Cochise Counties, Arizona
Plate 2.Complete Bouguer gravity anomaly map of the lower Cienega Basin area, Pima and Cochise counties, Arizona.
Plate 3. Aeromagnetic anomaly map of the lower Cienega Basin area, Pima and Cochise Counties, Arizona
Plate 4. Aeromagnetic map of the lower Cienega Basin area, Pima and Cochise Counties, Arizona.

LIST OF TABLES

Table 1. NURE aeromagnetic flight lines used to construct Plate 4
Table 2. Stations in and near the study area rejected from Roudebush [1996] data set
Table 3. Summary of physical properties used for geophysical modeling
Table 4. Basin thickness for several points along section B-B' in preferred and simple models.
Table 5. Summary of lithologic data from wells in the Cienega Basin area.

GEOLOGIC SETTING OF BASIN

The lower Cienega basin is located at the southern end of the Rincon Mountains in the hanging wall of the regional Catalina-Rincon Detachment fault (Figure 1, Plate 1). The basin records two major episodes of Tertiary sediment accumulation. Tertiary sediments were deposited on complexly deformed Precambrian granitic rocks, Paleozoic carbonate and clastic rocks, and Mesozoic igneous and sedimentary rocks. The first episode of sediment accumulation started about 30 Ma with deposition of conglomerate, sandstone, and locally mudstone of the Pantano Formation. Volcanic rocks are interbedded in this section near its base and in the middle part of the section. These strata were complexly faulted and tilted to dips of 10 to 70 degrees during movement on the Catalina-Rincon detachment fault. Strata of the Pantano formation are typically cut by numerous faults in outcrops in the eastern and western parts of the basin; the rocks range from strongly to moderately indurated. The Catalina-Rincon detachment fault is a large normal fault across which rocks in the Cienega Basin area have been transport 18-20 km to the southwest relative to crystalline rocks of the Rincon Mountains which form the footwall of the fault. These crystalline rocks are inferred to project beneath the study area. Pre-Tertiary rocks in the hanging wall of the detachment fault are strongly indurated, but highly faulted and fractured. Crystalline rocks beneath the detachment fault are probably considerably less fractured and faulted. The younger basin forming event largely postdates movement on the Catalina fault, and started after about 15 Ma. The younger basin was apparently bounded by north-trending normal

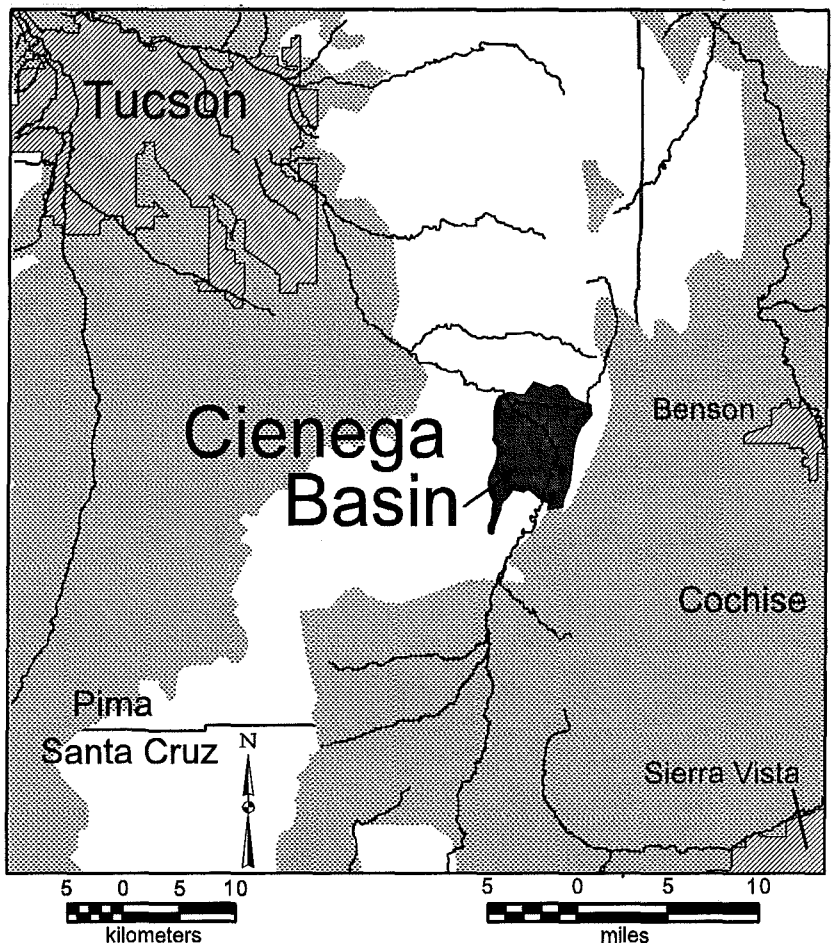

Figure 1. Location of Cienega basin study area. Shaded areas are alluvial basins; unshaded areas are bedrock outcrop areas

faults. Sediments deposited in this younger basin were referred to as Nogales formation by Drewes [1977]. They consist largely of sandstone and conglomerate, and are typically non-indurated to poorly indurated, and are cut by a few minor faults.

MAGNETIC DATA

Two magnetic data sets were used to constrain the subsurface geology beneath the Cienega Basin. Both are aeromagnetic surveys. The NURE (National Uranium Resource Evaluation) data were collected at an average elevation of 200 m along north-south flight lines, spaced about 5 km in an east-west direction. The Tombstone survey is an older data set, collected at a uniform barometric elevation of 9000 ft, along north-south flight lines spaced about 1.6 km in an east-west direction. The northern boundary of the survey is 32°N latitude, which passes through the northern part of the study area.

NURE data

Seven NURE flight lines traverse the study area. Several of the flight lines have a discontinuity at 32°N that probably separates data collected during different flights. Although the data are discontinuous at this boundary, the shapes of the profiles to the north and south match at the break, and can be aligned by adding a constant to either the data north or south of the discontinuity. Because SAKI shifts the average value of the calculated profile to match that of the data profile, addition of a constant value does not adversely affect the modeling. Correcting offsets were arbitrarily added to data north of 32°N latitude. Table 1 summarizes the offsets added to each data set. Section A-A' was located to follow the NURE flight line along longitude 110° 33' (line 130).

Table 1. NURE aeromagnetic flight lines used to construct Plate 4

Flight line	approximate W longitude	offset added north of lat. 32° (nTesla)	comments
125	110° 44'		no data north of 110.87°
127	110° 42'	34	
128	110° 39'	-58	
129	110° 36'	-38	
130	110° 33'	-172	0.4 km horizontal offset in flight lines at boundary
132	110° 30'	-14	1.3 km horizontal offset in flight lines at boundary
133	110° 27'	79	0.9 km horizontal offset 2.6 km north of boundary

Tombstone survey

The Tombstone survey was flown by the U. S. Geological Survey [Andreasen et al., 1965]. The data were obtained in digital form from Dr. M. Gettings at the USGS Tucson Field Office. These data were gridded using Surfer® (v. 6), with the minimum curvature algorithm. The contour map so obtained closely matched the published contour map included in Andreasen et al. [1965].

GRAVITY DATA

Gravity data were compiled by E. Roudebush as part of a M.S. thesis [Roudebush, 1996] in hydrology at the University of Arizona, Tucson. This data compilation includes data from several sources, including USGS data, data collected by Ellett [1994] and Roudebush [1996]. The data were gridded using Surfer® (v. 6), with the minimum curvature gridding algorithm. Residuals (the difference between the grid value and measured value) at each gravity station were calculated, and stations for which the residual was greater than 1 mgal were examined to determine the reason for discrepancies. This analysis resulted in the rejection of 7 stations which were found to differ by >2mgal from other nearby stations, resulting in unreasonably large gravity gradients (see Table 2). The principal effect of this data screening is that the gravity low indicated by Ellett [1994] near 31° 57'N 110°34'W is greatly reduced in amplitude, with the result that the sub basin modeled in this area is much shallower than in Ellett's [1994] model (compare his section D-D' with section C-C' in this report).

Table 2. Stations in and near the study area rejected from Roudebush [1996] data set

ID	latitude	longitude	altitude (ft)	Bouguer anomaly	residual
5918T215	32.0863	-110.6270	3541.2	-120.95	2.424
5918RV	32.0117	-110.7033	3490.3	-113.86	-0.529
E97	31.9140	-110.5805	4417	-132.88	4.784
5918N-23	31.8837	-110.4258	4600.3	-125.47	1.236
5918N-11	31.8268	-110.4870	4850.3	-132.93	0.303
5918N-14	31.8210	-110.4598	5340.2	-131.32	-2.168
3138E045	31.7883	-110.6333	4539.9	-148.52	not calculated

SAKI

Forward modeling of gravity and magnetic fields was done using the program SAKI [Webring, 1985]. This software is freely available from the US Geological Survey. The DOS version of the program was used. Geologic cross sections must be entered in a coordinate system with the origin at sea level at one end of the section line, elevation measured positive downward (i.e. negative elevations are above sea level), and in units of kilometers only. The geometry is defined by the X-Z coordinates of numbered vertices along the boundaries of the rock units in the cross section (see appendix I). The program allows interactive editing of several parameter values, including x and z coordinates of vertices, density, susceptibility, and magnetization of each body. Varying the length of each body normal to the section line allows some compensation for bodies that are not symmetrical across the cross section plane. No magnetization data were available for rock units in the study area, so all magnetization values (intensity and orientation) have been set to 0.

PHYSICAL PROPERTIES OF ROCKS

Density and susceptibility values for the geological models were compiled from the literature [Bankey and Kleinkopf, 1985; Bittson, 1976; Dietz, 1985; Ellett, 1994; Greenes, 1980; Halvorson, 1984; Tucci et al., 1982]. Table 3 summarizes the density and susceptibility values used in the models included here. Note that the density contrasts for the bedrock units (those other than QTg and Tp) are typically an order of magnitude lower than those for the Tertiary-basin-filling units. All sedimentary rocks have been assumed to have

Table 3. Summary of physical properties used for geophysical modeling

rock unit	density contrast				susceptibility		
	min	max	avg	preferred	min	max	avg
QTg	-0.515	-0.300	-0.426	-0.5	0	0	0
Tp	-0.500	-0.250	-0.309	-0.3	0	0	0
Ke	-0.031	-0.007	-0.018	-0.02 to -0.07	0.0010	0.0034	0.0026
Kb	-0.077	-0.002	-0.045	-0.07	0	0	0
Kbg	-0.050	0.041	0.009	0.02-0.05	0	0	0
MYu	-0.012	0.110	0.039	0.03-0.07	0	0	0
YXu	-0.086	0.050	-0.034	-0.02 to -0.07	0.0007	0.0054	0.0024
YXu + Tg	-0.060	-0.015	-0.038	-0.02 to -0.07	0.0001	0.0032	0.0020

Density contrasts are based on a reference density of 2.67 g/cc. Rock unit abbreviations are defined in the explanation for cross sections (Figure 2)

no magnetic susceptibility. This assumption is probably not true for volcanic rocks associated with the Pantano Formation (Tp) and in the upper Cretaceous part of the section. The Pantano volcanic rocks are too small in volume along the section lines to produce a discernible effect in the Tombstone magnetic survey data, which was flown at a relatively high altitude (about 6500 feet (2000 m) ground clearance). The Cretaceous volcanic rocks crop out too far from the section lines to have and effect. Remnant magnetization in these units has also been assumed insignificant.

Map Units in Cross Sections

Quaternary and Tertiary

QTc conglomerate

Miocene and Oligocene

Tp Pantano Formation, undivided

Cretaceous

Ke quartz monzonite of Empire Mountains

Kb Bisbee group, undivided; sandstone, shale, conglomerate and sparse limestone

Kbg Glance Conglomerate member; basal conglomerate of Bisbee group

Middle Proterozoic, Paleozoic and Lower Mesozoic

MYu Apache Group, Bolsa, Abrigo, Martin, Escabrosa, Horquilla, Earp, Colina, Concha, Sherrer, Epitaph, Rainvalley and Gardner Canyon formations, undivided; quartzite, limestone, dolomite, sandstone and shale

Proterozoic

YXu granitic and metamorphic rocks undifferentiated

YXu+Tg undivided Proterozoic granitic and metamorphic rocks and early Tertiary Wrong Mountain granite, in footwall of Catalina-Rincon detachment fault

Figure 2. Explanation of unit abbreviations used on cross sections.

Discussion of Cross sections

Four cross sections were constructed--one north-south (A-A') and three east-west (B-B', C-C', D-D'). The sections were initially drawn based on analysis of the geologic map data. These sections were converted into SAKI models (see above and Appendix I) to use as the starting point for modeling the observed gravity and magnetic fields. Figure 2 summarizes the abbreviations used for map units on the cross sections.

Section A-A'

Section A-A' is a north-south section through the central part of the basin (Figures 3 and 4), drawn along one of the NURE aeromagnetic lines in order to take advantage of this data for basin modeling. High frequency variations in the magnetic anomaly were recorded just north of 32° N and at the northern end of the section. The

32° N anomaly is located where the section line crosses I-10 and the Southern Pacific Railroad, and is likely the result of a railroad train. The rapid variations at the northern end of the line are interpreted to result from ground clearance variations as the aircraft collecting the data flew over the rugged terrane at the southern end of the Rincon Mountains. There is no evidence of the variation in rock types at the surface that would be necessary to produced this kind of variation [Drewes, 1977]. The susceptibility of the footwall rocks (body19, unit YXu + Tg) was adjusted to obtain the best fit possible with these high frequency variations. The final fit (Figure 3) is not especially good, probably because of the steep terrain and significant local relief on the south flank of the Rincon Mountains. The principal feature of the magnetic model and a north to south decrease in field strength interpreted to reflect increasing depth to the Catalina-Rincon Detachment fault, which is modeled as the top of magnetic basement. The steepness of the magnetic gradient, in combination of the susceptibility estimated for rocks below the fault requires that the boundary steepen dramatically between 8 and 9 km south of the north end of the line. Based on the northeast trend of this gradient in map view (plates 3 and 4), this zone is interpreted to trend northeast, probably representing a tear fault or lateral ramp in the detachment fault system.

The northern end of section A crosses the Catalina-Rincon Detachment fault, north of which rocks of the Wilderness granite and Oracle Granite crop out along the section line. Unfortunately, no gravity stations constrain the gravity field north of where it crosses the detachment fault. The gravity gradient onto the footwall of the detachment fault is thus very poorly constrained and does not provide a means of estimating the density contrast for the footwall.

The gravity anomaly over the main part of the lower Cienega basin is characterized by a relatively gentle gradient without dramatic changes in slope. This suggests that the low density fill in the basin has relatively gently dipping margins. Subtle changes in the gradient probably represent structure beneath the low density fill, interpreted here as fault blocks above the Catalina-Rincon detachment fault containing thicker accumulations of Pantano Formation in their hanging wall blocks. The section is sub-parallel to the northerly trend of normal faults expected to cut the Pantano Formation based on its structure in outcrop south and west of the basin. These faults would be expected to intersect the section line at a low angle and be poorly resolved by the gravity data. The northwestern boundary of the bedrock high that trends north from the vicinity of the Narrows along Cienega Creek is interpreted to underlie the steeper gradient observed at the south end of the gravity low associated with the basin. A more subtle increase in slope about 3 km to the north is interpreted to reflect thickening of Pantano formation across an ENE trending boundary zone active during deposition of the Pantano Formation.

Section B-B'

Section B-B' crosses the central part of the Cienega Basin from east to west (Figures 5 and 6). The eastern end of the section is the bedrock high that defines the eastern boundary of the lower Cienega Basin. Bedding orientation in Pantano Formation on the flanks of this bedrock high define an antiform, but the Pantano Formation does not form a continuous belt to define a fold; in addition, bedding orientation in the Bisbee formation in this structural high do not suggest that the Bisbee has been folded. This structural high appears to be a horst with bedding in the hanging wall of bounding normal faults dragged to dip in the same direction as the faults. Northerly trending normal faults bound blocks of east tilted Pantano Formation at the western end of the line.

The section is oblique to the strong magnetic gradient related to the Catalina-Rincon Detachment fault (see discussion of section A above). The Tombstone survey was flown at too high an altitude to measure anomalies related to volcanic rocks interbedded in the Pantano Formation. The available magnetic data is thus not very useful for defining Cienega basin geometry.

The absence of significant gradients along the western part of the line apparently indicates that the depth to magnetic basement is relatively constant along the section. The modeled depth to magnetic basement, again interpreted to represent the Catalina-Rincon detachment fault in the eastern half of this section line,

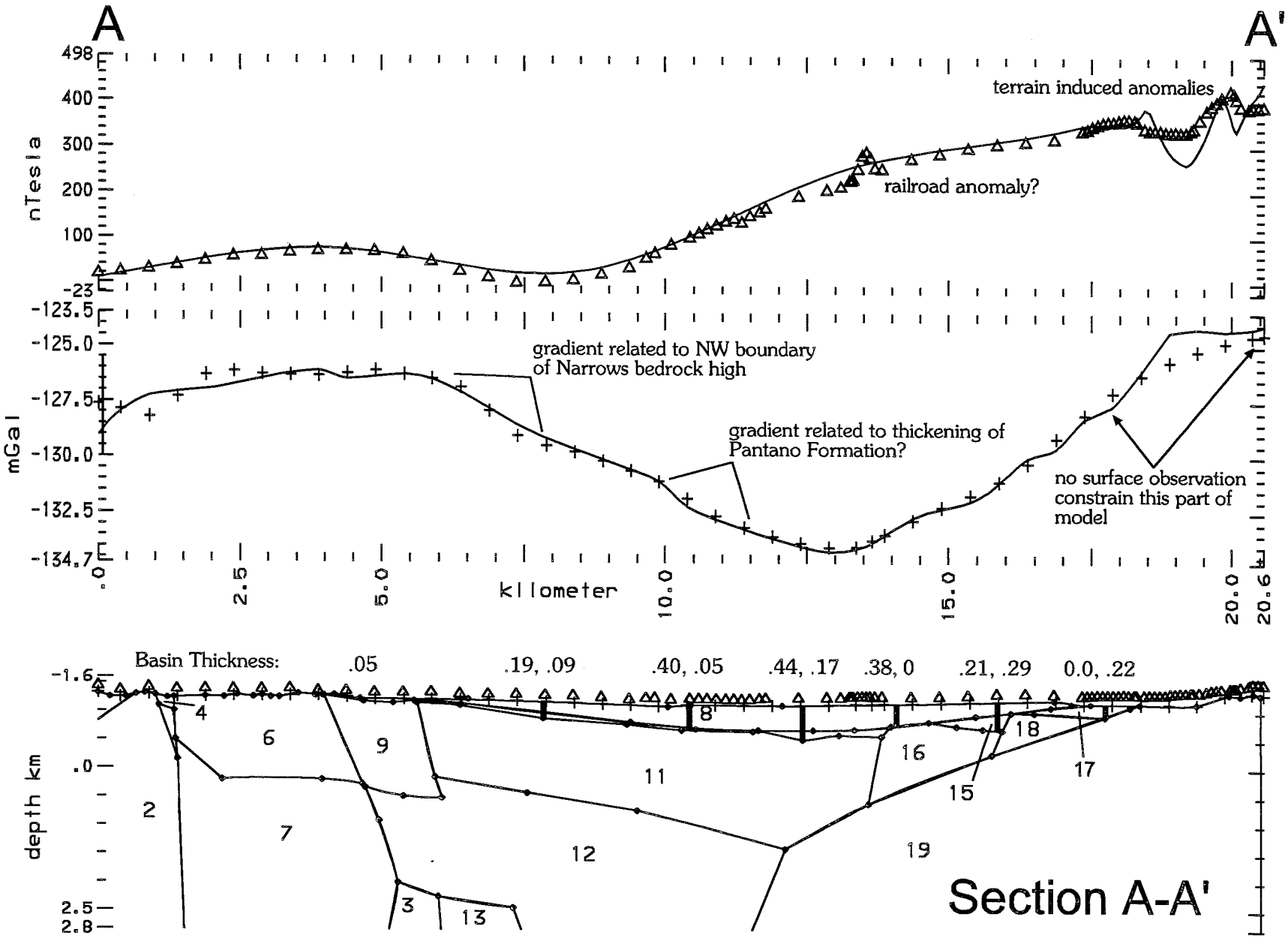

Figure 3. Cross section models and calculated gravity and magnetic anomalies for section A-A'

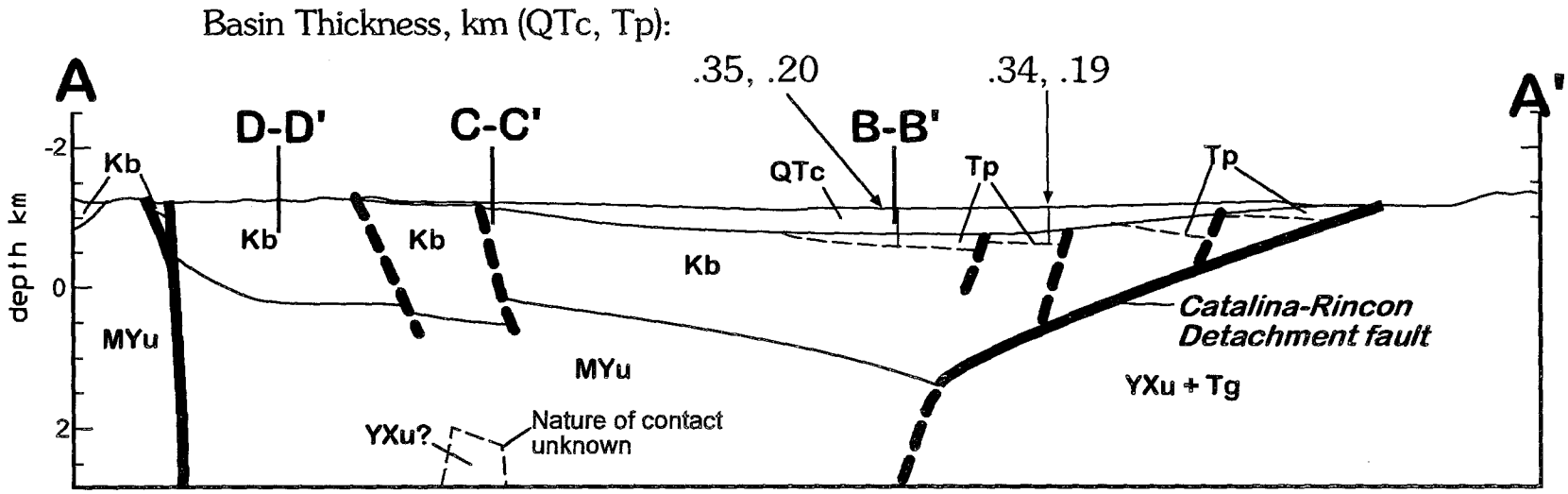

Figure 4. Geologic cross section A-A'

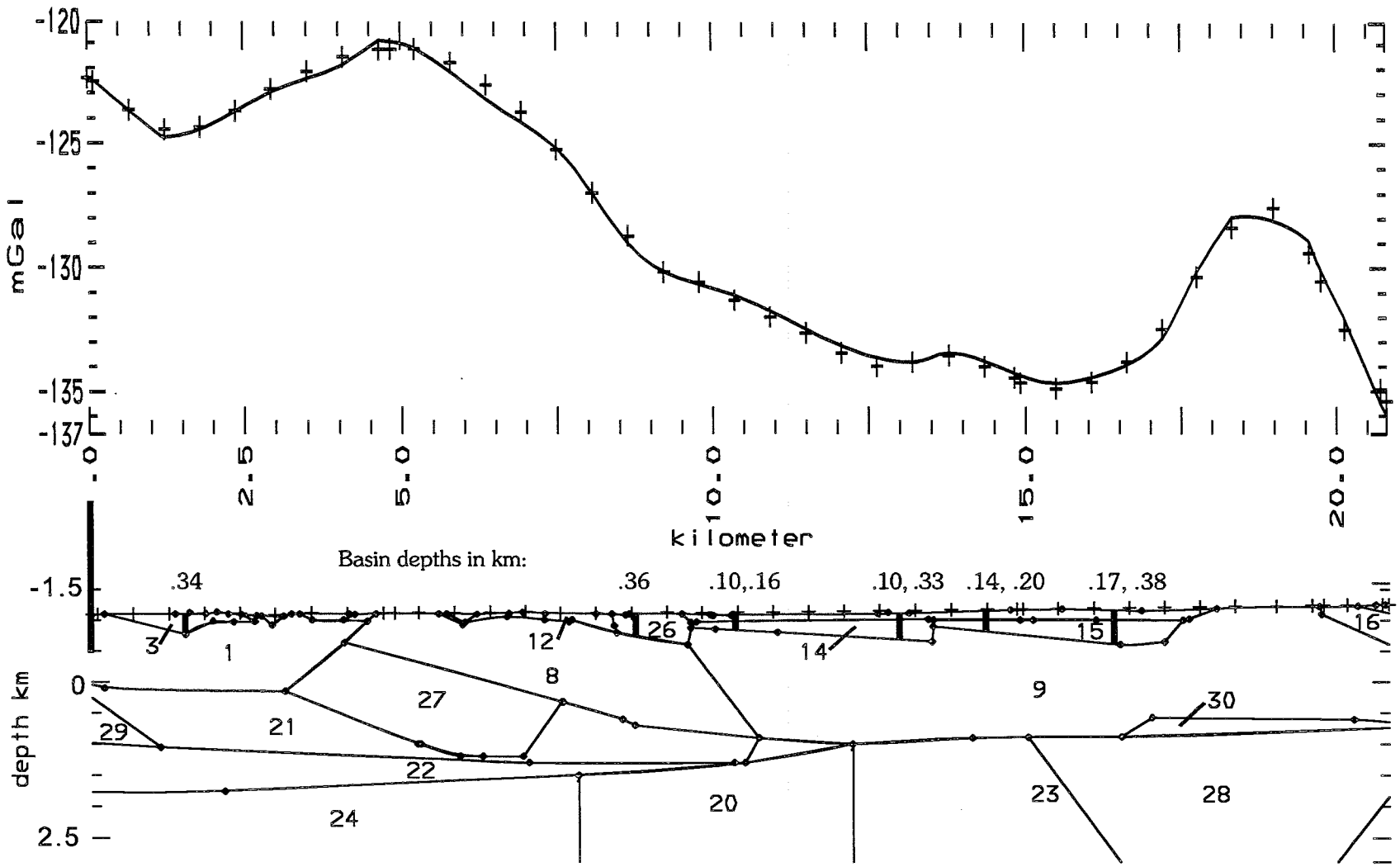

Figure 5. Cross section models and calculated gravity anomaly for section B-B'

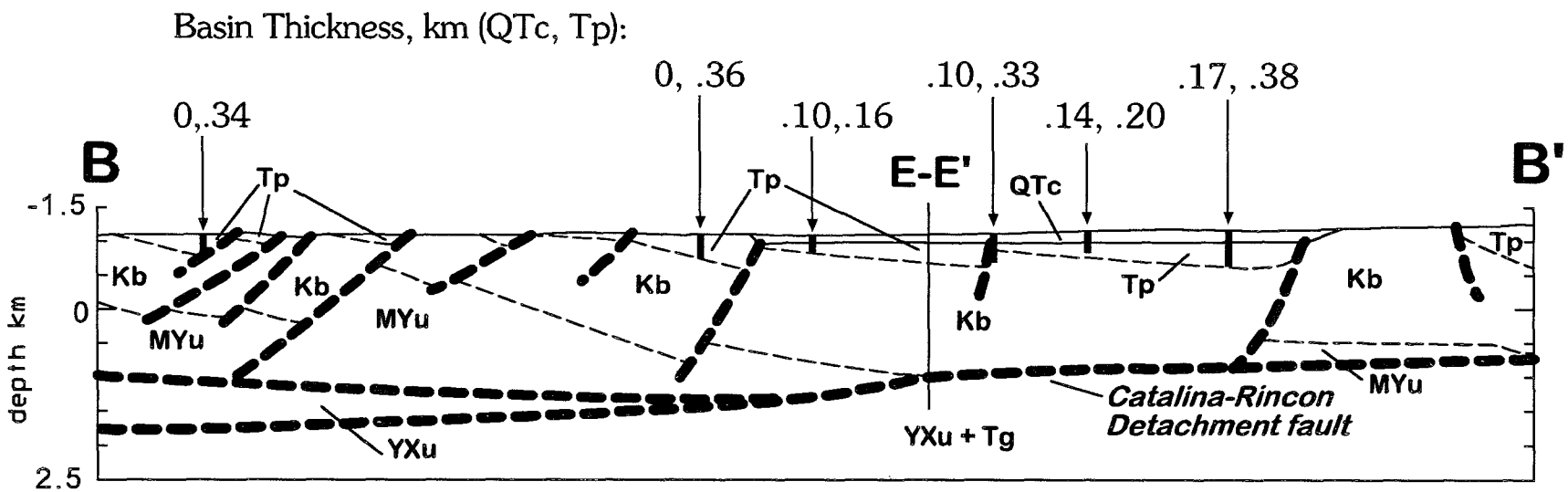

Figure 6. Geologic cross section B-B'

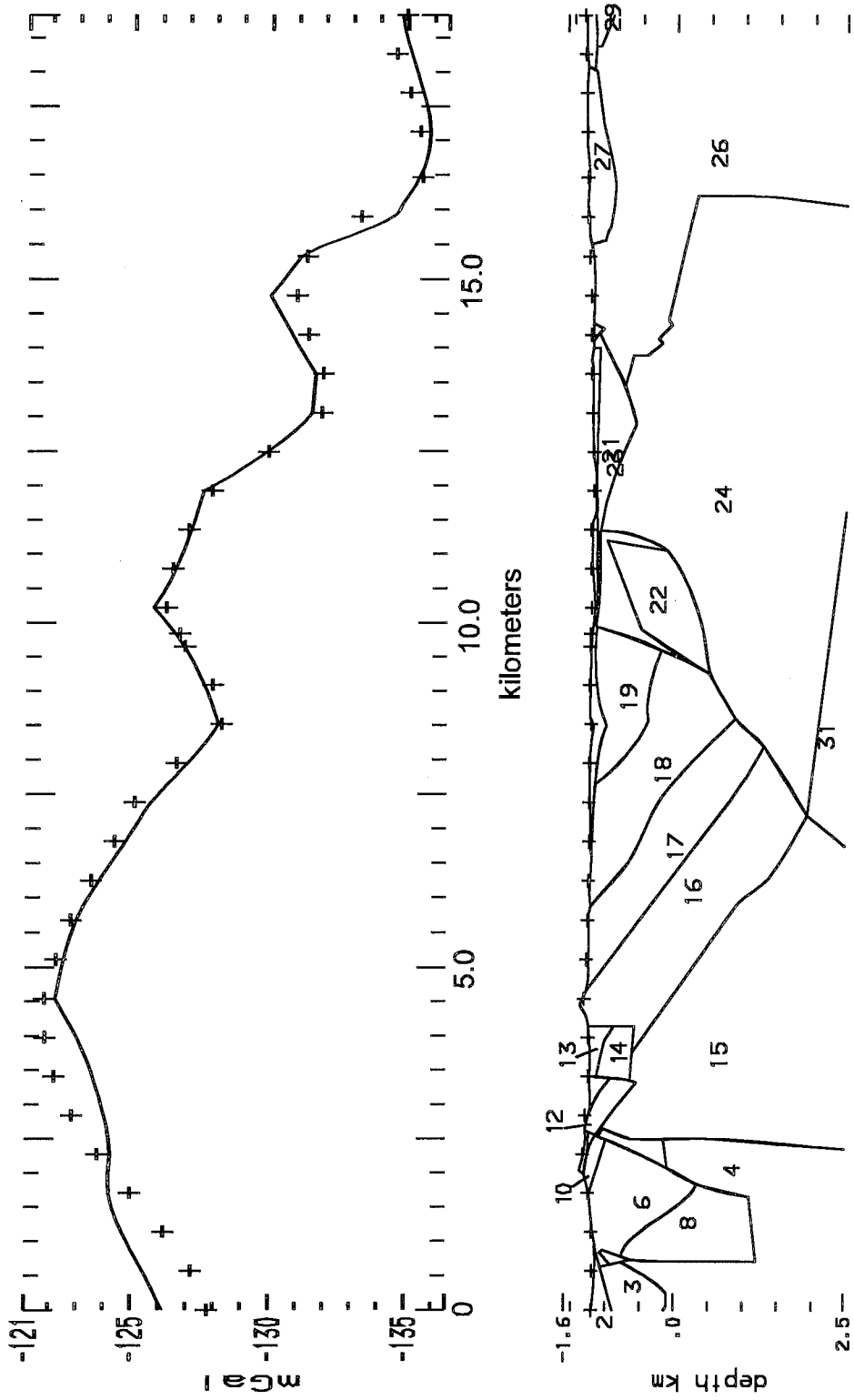

Figure 7. Cross section models and calculated gravity anomaly for section C-C'

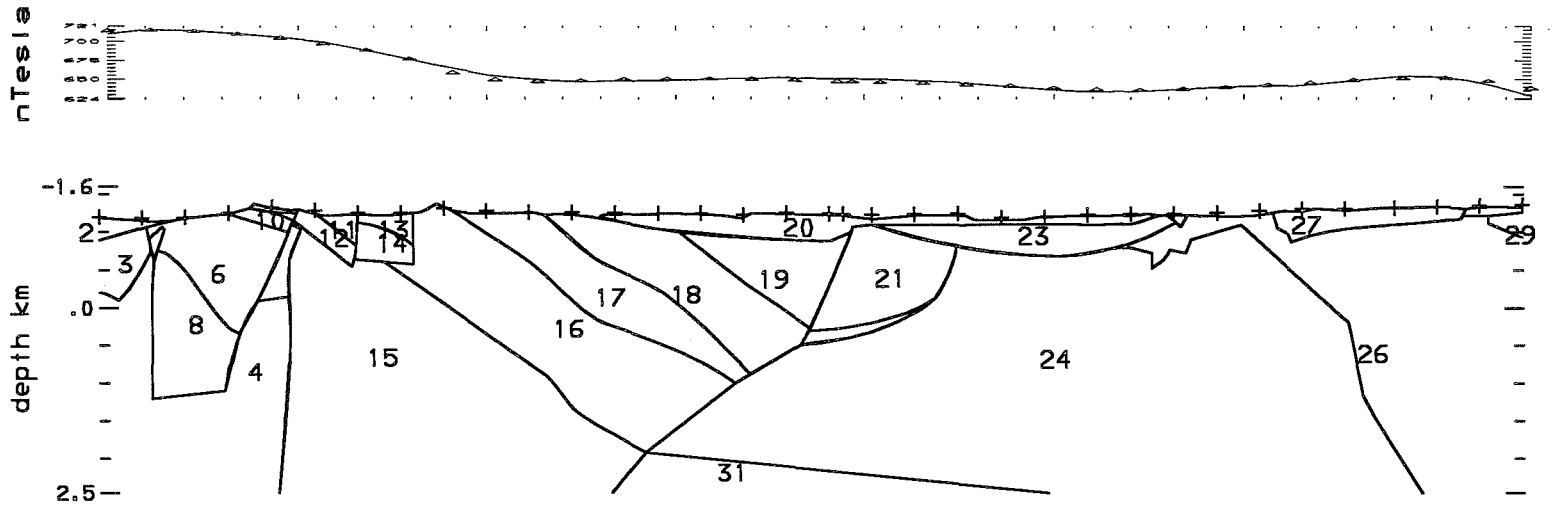

Figure 8. Cross section models and calculated magnetic anomaly for section C-C'

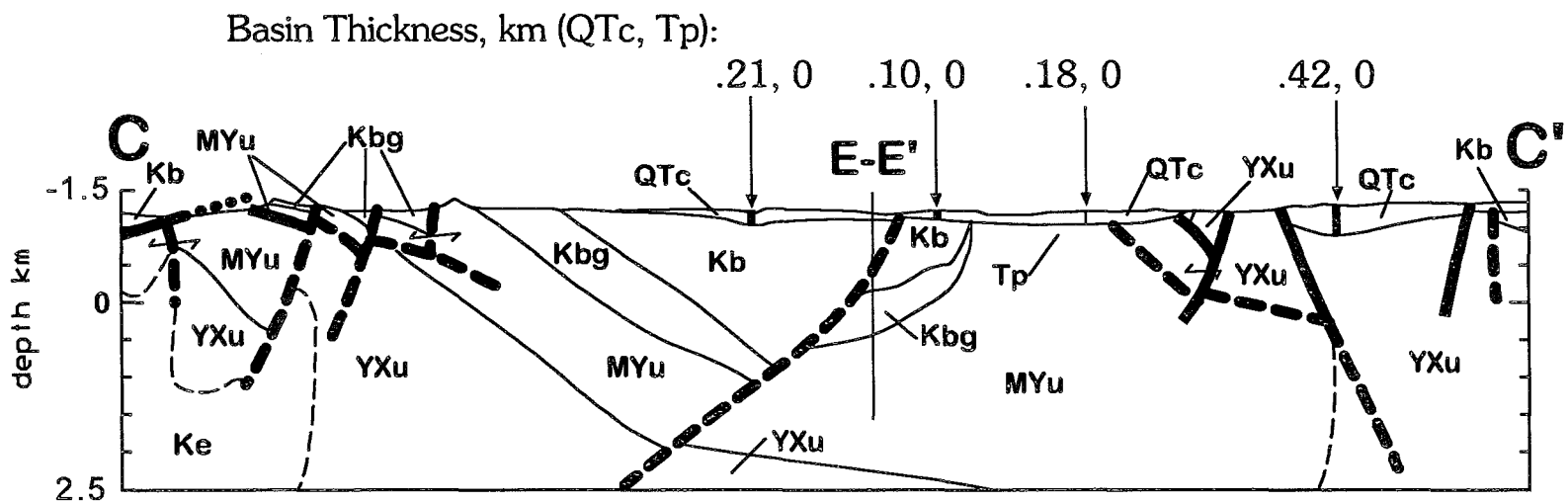

Figure 9. Geologic cross section C-C'

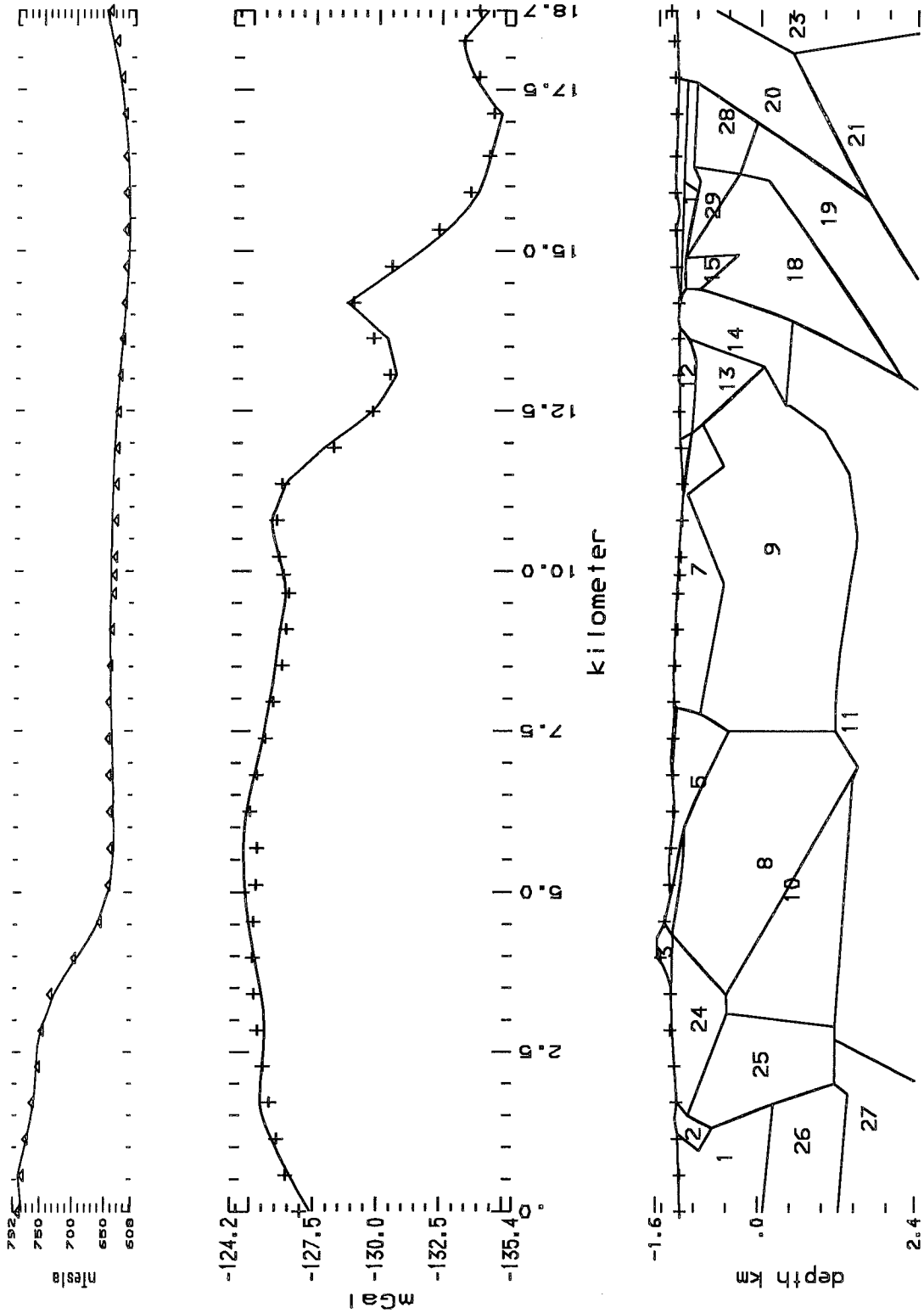

Figure 10. Cross section models and calculated gravity and magnetic anomalies for section D-D'

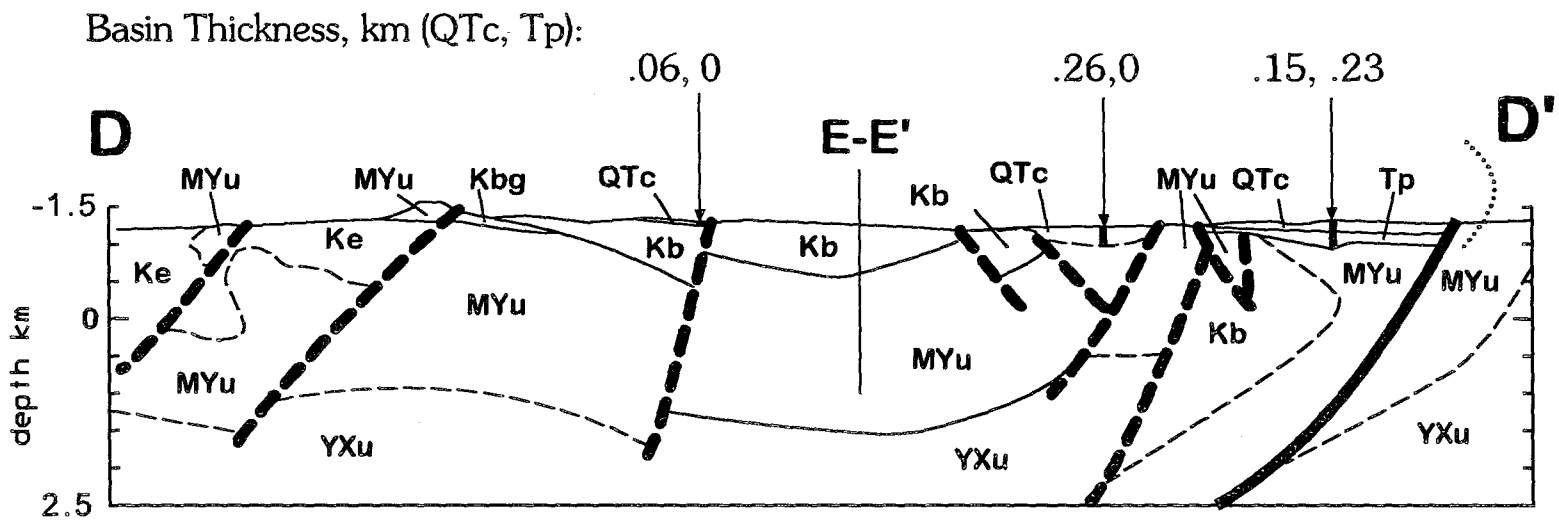

Figure 11. Geologic cross section D-D'

does not agree well with the depth where this line crosses section A. This is probably due to the fact that the section intersects the magnetic anomalies and geologic structure at a low angle. Along the western half of the line, interpretation of the magnetic anomalies is further complicated by the structurally high mass of Proterozoic granite in the core of the large east-trending fold, which is subparallel to the section on the south side. Depth to magnetic basement along this line is poorly constrained.

The gravity anomaly includes three major features. A broad high on the western part of the section reflects proximity to bedrock of the Empire Mountains. A broad low in the central part of the line reflects low-density sediment in the main Cienega Basin. A narrow gravity high at the eastern end of the line reflects the bedrock ridge that forms the eastern boundary of the Cienega basin.

Several off-axis bodies have been used in this model to account for the asymmetric distribution of rock units along the section line. Pantano formation in tilted fault blocks along the section line is truncated along a WNW trending fault zone within about 1 km south of the section line, but continues for 4-5 km north of the section line. These tilted fault blocks of Pantano Formation do not produce a discernible gravity anomaly. The 3 to 4 mgal low at the western end of the line corresponds to a largely inferred Pantano fault block, but the anomaly probably reflects a thin layer of QTg exposed at the surface. The general lack of gravity anomalies corresponding the outcropping structure is interpreted to indicate a minimal density contrast between well indurated Pantano formation and lithologically similar underlying Bisbee Group sediments in this area.

Relatively steep gradients along the boundaries of the main gravity low associated with the basin suggest that these boundaries are steep and especially on the eastern side, probably related to normal faults. The broad gravity low has been modeled with a layer of low-density QTg, and slight modulation of this anomaly has been modeled with underlying tilted blocks of Pantano formation. Lithologic and diagenetic variations in Pantano formation could easily produce significant density variations. Thus, the relative thickness of QTg and Tp is not well constrained (compare Sections A and B where they cross).

Section C-C'

The magnetic anomaly profile along section C-C' exhibits a board high on its west end related to structurally high Cretaceous granite (Ke) and Proterozoic crystalline rocks (YXu) (Figure 7). The magnetic field strength decreases off this high to the east as magnetic basement gets progressively deeper in the east-dipping Empire Mountains tilt block. The eastern part of the section is subparallel to the large fold structure inferred in units YXu, MYu, and Kb, and the magnetic data is only marginally useful in this area for determining depth to bedrock. A slightly different model was used for modeling the magnetic and gravity anomalies mostly in an attempt to account for this structure. At the eastern end of section C-C', basin fill QTg is deposited directly on Proterozoic crystalline rocks, and magnetic basement corresponds with bedrock defining the basin. In this case the magnetic depth to bedrock was interpreted to be reliable and was used to estimate the density of YXu underlying the sub basin between the bedrock high forming the eastern margin of the Cienega basin and Whetstone Mountains.

The gravity anomaly profile is dominated by a west-to east negative slope (Figure 8), modulated by three anomalies with wavelengths of about 5 km. These anomalies are related to sub-basins in the zone separating the Cienega and Sonoita basin. The easternmost of these sub basins is east of the bedrock high that forms the eastern boundary of the Cienega Basin, and is thus a separate small basin. As mentioned above, the magnetic data constrain the depth to bedrock relatively well in this sub-basin.

Pantano Formation strata dip steeply west on the west side of the Cienega basin-bounding bedrock high. A tuff present at the base of this section resembles tuff near the base of the Pantano Formation (Tp) section at the north end of the Empire Mountains, suggesting that this steeply tilted strata is near the base of the Tp. Thus the central sub-basin has been modeled with a significant thickness of Tp, probably in complexly faulted blocks. The lower density contrast between Tp and bedrock results in a greater thickness of Tp required to produce the observed anomaly than if the basin fill were lower density QTg. Thus the central sub-basin appears deeper than the other two sub-basins in this section (Figure 9).

Section D-D'

Section D-D' is located at the south end of the Cienega basin (Plate 2), in the zone linking it with the Sonoita basin to the south. The section was constructed with hopes that bedrock geology from this section could be projected down dip beneath the basin. It soon became clear that because of easterly trending pre-Tertiary structures, such projection is not really possible.

The magnetic anomaly profile (Figure 10) is quite similar to that along section C-C', with the exception that the gradient off the bedrock of the Empire Mountains is much steeper due to the presence of bodies of Cretaceous granite intruding Paleozoic rocks. The flat central part of the profile indicates little relief on the magnetic basement in this area. The slight increase in field intensity at the east end of the profile is related to the southeast-dipping contact between non-magnetic Paleozoic strata and underlying Proterozoic crystalline rocks, which crop out just east of the eastern end of the profile (Figure 11).

The gravity anomaly profile is relatively flat over the bedrock units in the western two thirds of the section, reflecting the relatively small density contrasts between the rocks in this area. A generally negative slope at the eastern end of the line suggests that the Proterozoic crystalline rocks cropping out in the Whetstone Mountains have a lower density that the basement rocks in the Empire Mountains. Two gravity lows superimposed on this part of the profile are related to two sub-basins that are the southern continuation of the central and eastern sub-basins in profile C-C'.

EVALUATION OF MODELING PROCEDURE

Two experiments were run to investigate the usefulness of modeling sub-basin geology. First, the gravity anomaly data were modeled with a single body representing Tertiary sedimentary rocks (Tp and QTg undifferentiated). The model included five bodies, representing the Tucson basin, San Pedro Basin and two sub-basins in the Cienega Gap area (Figure 12). The western sub-basin represents the tilted fault blocks of Pantano formation along the western part of the section line. The other sub-basin is the main Cienega basin.

Two models were made for the basins in the Cienega gap area, one with a density contrast of -0.5 and one with a contrast of -0.2. The lower contrast represents basin fill density of 2.2 g/cc and the underlying bedrock (Bisbee formation) density of 2.4 g/cc, figures chosen to represent a minimum reasonable contrast between basin and bedrock. The higher contrast represents basin fill density of 2.17 g/cc and bedrock with a density of 2.67 g/cc, representing a relatively high contrast. A density contrast of -0.5 g/cc was used for the San Pedro and Tucson basins in both models. These models predict upper and lower bounds for basin depth of about 2.1 and .55 km (6800 feet and 1800 feet)

In both cases it was impossible to model the gravity highs in the observed data. Insufficient density contrast could be obtained to match the broad high at the western end of the section, and a mass excess below the bedrock high on the eastern side of the basin resulted in calculated gravity values being too high at the eastern end. The discrepancy between the data and the simple models is consistent with a regional east to west gradient of about 0.3 mgal/km. This gradient is very similar in magnitude to that expected due to the regional isostatic anomaly related to crustal thickening towards the Colorado Plateau [Aiken, 1976; Simpson et al., 1986]. This observations suggests that if isostatic residual gravity values were used, the basin anomalies could be well modeled with a single body representing the basin.

The second test run to investigate the sensitivity of the basin model to the sub-basin geology model was to compare the anomalies due solely to the Tertiary basin fill units (Tp and QTg) and the anomaly due to the basement units (all others) in the final basin model for section B-B' (Figure 13). The broad high-low-high pattern of the observed data is reflected in both anomalies, but the bedrock anomalies are smoother, due to deeper source and lower density contrasts. Steeper gradients in the observed gravity are clearly modeled by the near surface, low density basin fill units as expected.

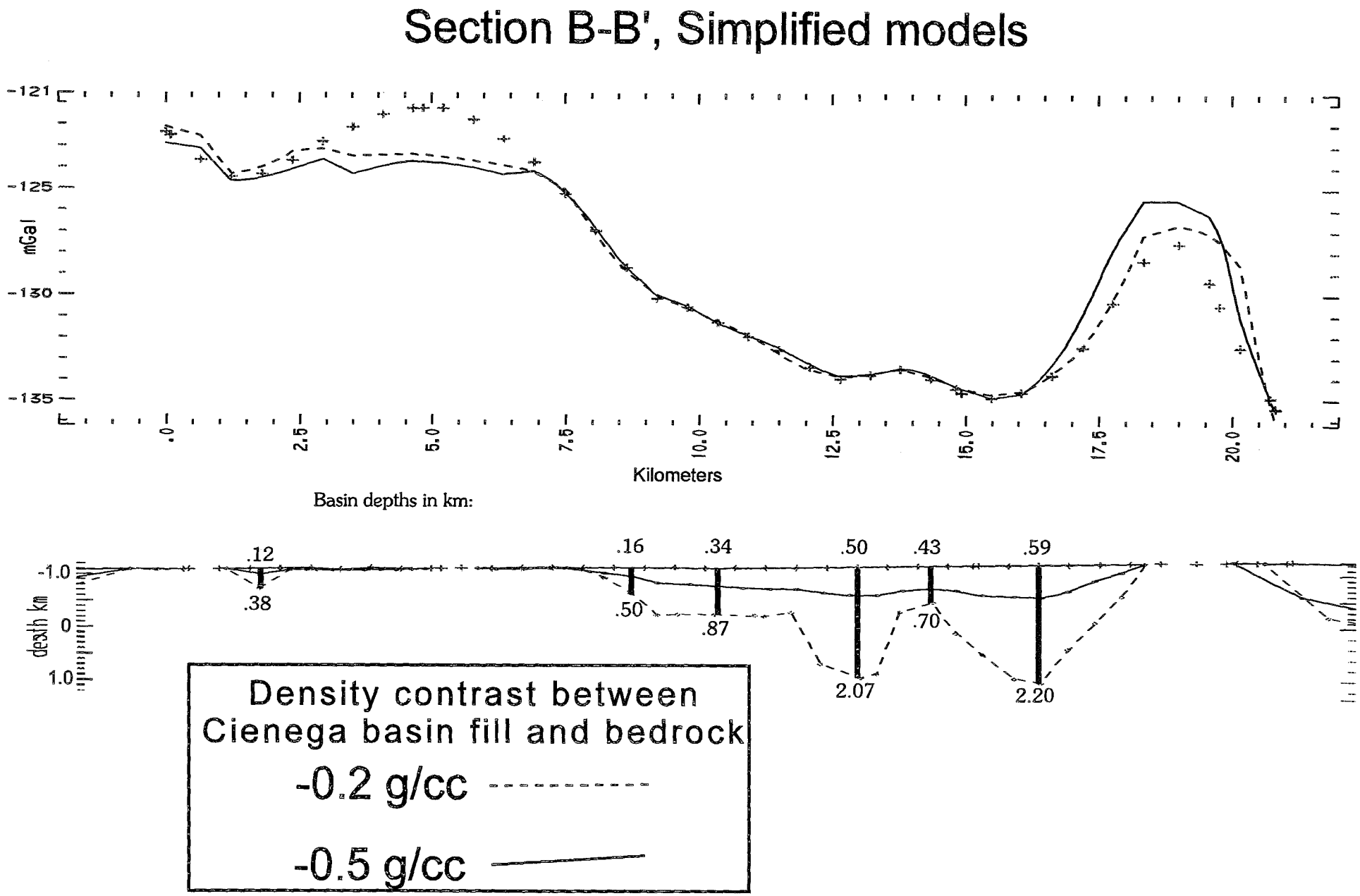

Figure 12. Simplified gravity model for section B-B'

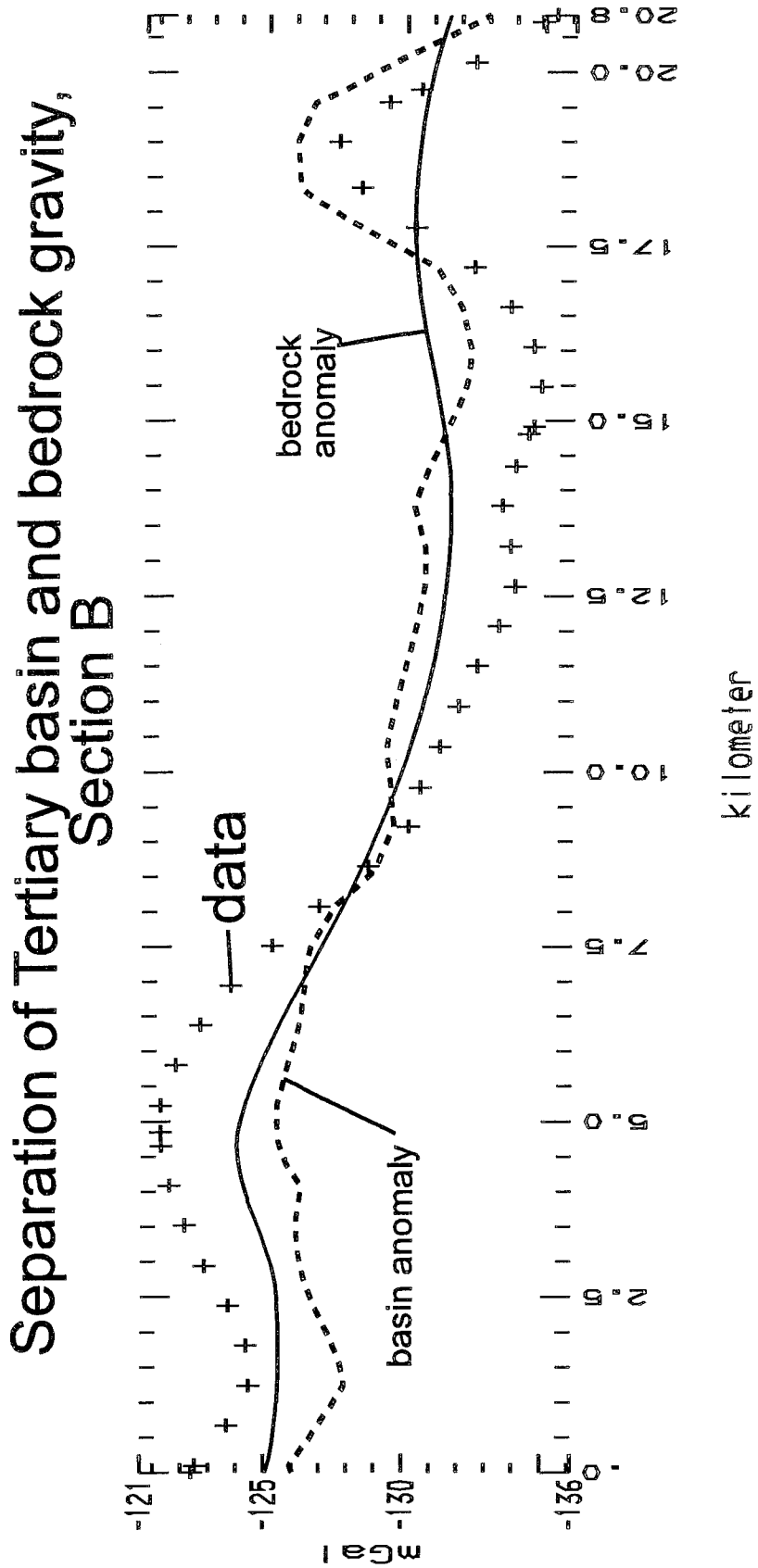

Figure 13. Separation of anomalies due to basin fill units (Tp and QTg) and bedrock units.

Table 4. Basin thickness for several points along section B-B' in preferred and simple models.

Preferred model (km)			Simple model (km)	
QTg	Tp	sum	min	max
	.34	.34	.12	.38
	.36	.36	.16	.5
.10	.16	.26	.34	.87
.10	.33	.43	.50	2.07
.14	.20	.34	.43	.70
.17	.38	.55	.59	2.20

The basin thickness (QTg +Tp) has been determined in both the simple and full models at several points along section B-B' (Figure 12, 5, 6). In the main Cienega basin, the full model consistently predicts shallower depth to bedrock than the high contrast (-0.5 g/cc) simple model. Examination of the separated bedrock and basin fill anomalies (Figure 13) explains this relationship. Because part of the gravity low associated with the basin is accounted for by density variations in the bedrock in the full model, less basin fill is required to produce the full anomaly.

Thus it appears that in order to bound the thickness of basin fill, a simple model with the lowest reasonable density contrast between the basin fill sediment and underlying bedrock suffices to determine an upper bound on basin thickness. Establishing a lower bound requires consideration of the bedrock geology to determine how much of the gravity low associated with the basin might be related to bedrock density variations. In either case, removal of a regional isostatic anomaly is necessary to produce the most accurate estimates.

GEOLOGIC SYNTHESIS

Mesozoic structures

A Glance-Conglomerate-age (late Jurassic or early Cretaceous) structure trends easterly through the north central Empire Mountains. South of this structure, Glance conglomerate is thick and is deposited on upper Paleozoic or lower Mesozoic strata (Figure 14). North of a complex fault zone, the Glance conglomerate is thin or absent and Bisbee Group strata are deposited directly on Proterozoic crystalline rocks. When Paleozoic rocks appear again in the Colossal cave area northwest of the Cienega basin, upper Proterozoic Apache group strata (absent in the Empire Mountains) are present between the basal Cambrian quartzite and Proterozoic crystalline rocks (see Drewes [1977]). The relationship of Proterozoic crystalline rocks in the Colossal cave area to those underlying Bisbee Group strata in the northern Empire Mountains is unknown. If they are structurally continuous, they would be part of a large Glance-age north-tilted structural block. The southern boundary of this block is a zone of complex faulting. The major structures appear to be gently to moderately north-dipping thrust faults. Given the complex history of this area, the faults that now bound the northern Empire Mountains block are likely to be younger structures that largely excise the original boundary (e.g. thrust faults related to the fold described below). This boundary can be traced east to the bedrock high that forms the eastern boundary of the Cienega basin. Its location east of there is ambiguous, but must lie in or north of the northern Whetstone Mountains.

Much of the Bisbee group under and adjacent to the main Cienega basin is steeply dipping to overturned (Figure 14). These dipping beds are apparently involved in large-scale folds that involve the entire Bisbee group, which is clearly younger than the Glance-age structure described above. These folds are most probably related to middle or late Cretaceous in age (Laramide?) contraction.

Figure 14. Mesozoic structural and stratigraphic features of the Cienega Gap study area. Stippled area is pre-Tertiary bedrock outcrop. Strike and dip data are for Bisbee Group strata. Base map is portion of base map used for Plate 1. Scale 1:100,000 (same as plates).

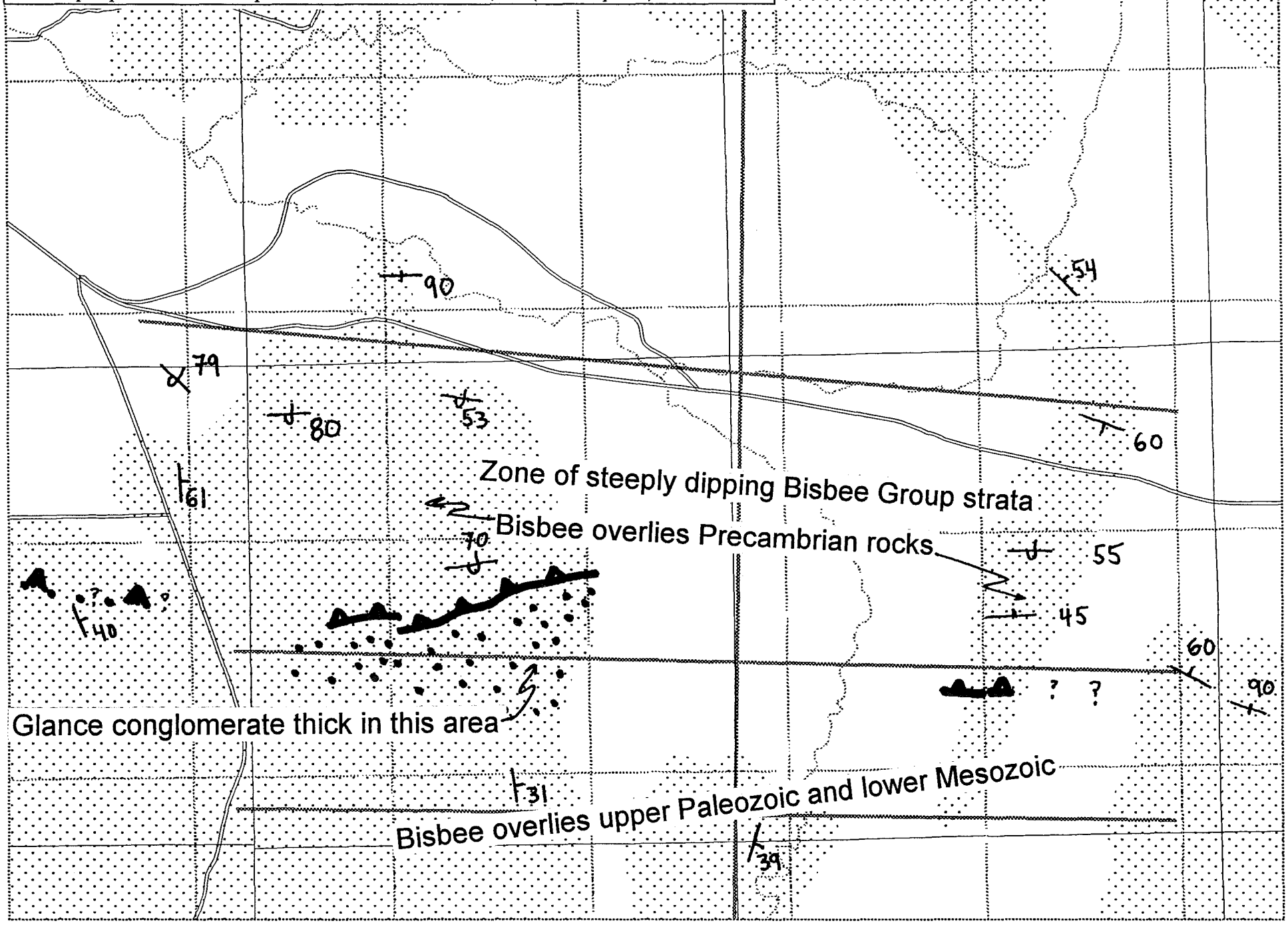

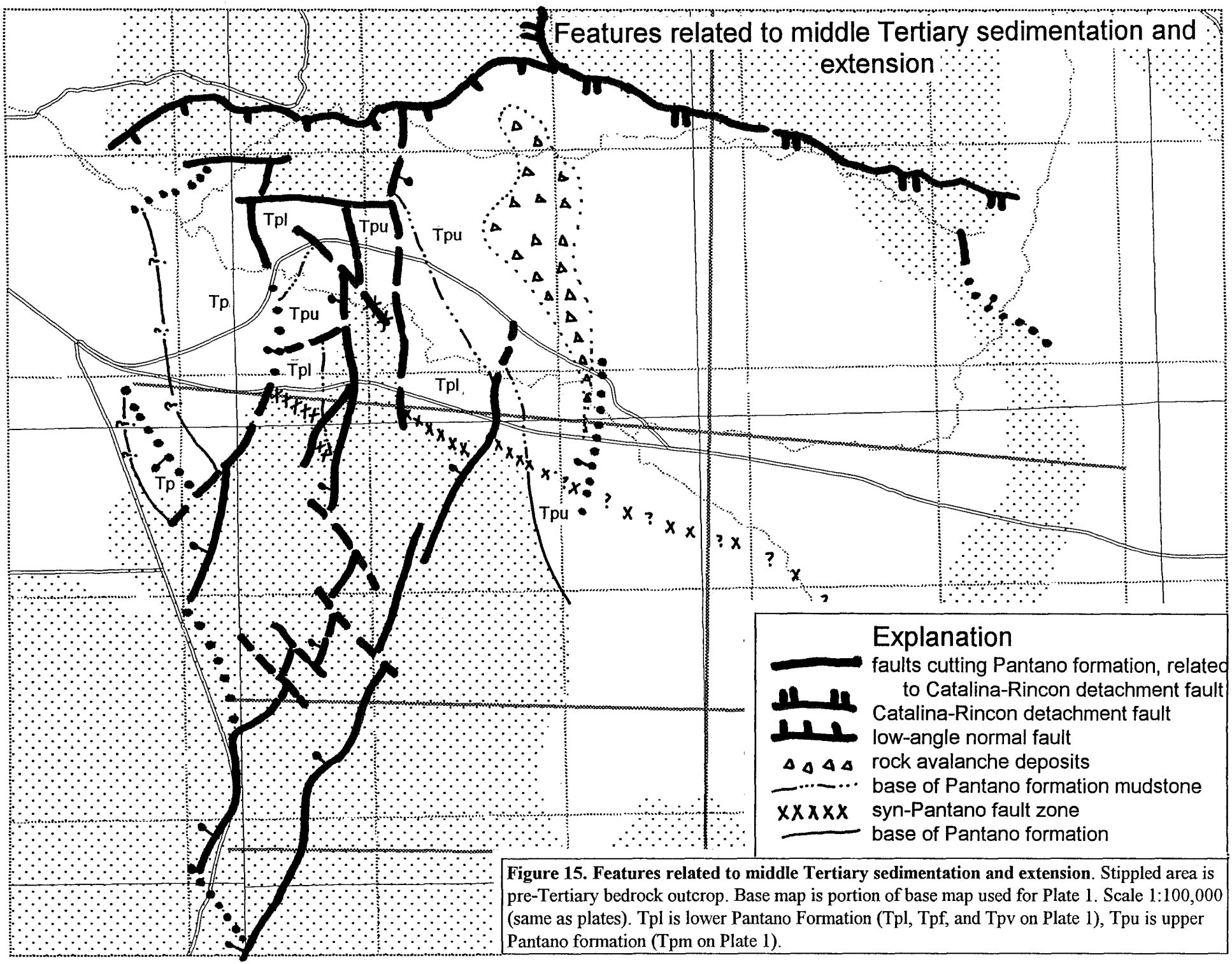

Figure 15. Features related to middle Tertiary sedimentation and extension. Stippled area is pre-Tertiary bedrock outcrop. Base map is portion of base map used for Plate 1. Scale 1:100,000 (same as plates). Tpl is lower Pantano Formation (Tpl, Tpf, and Tpv on Plate 1), Tpu is upper Pantano formation (Tpm on Plate 1).

Figure 16. Younger basin-fill related sedimentation and structure. Stippled area is pre-Tertiary bedrock outcrop. Base map is portion of base map used for Plate 1. Scale 1:100,000 (same as plates).

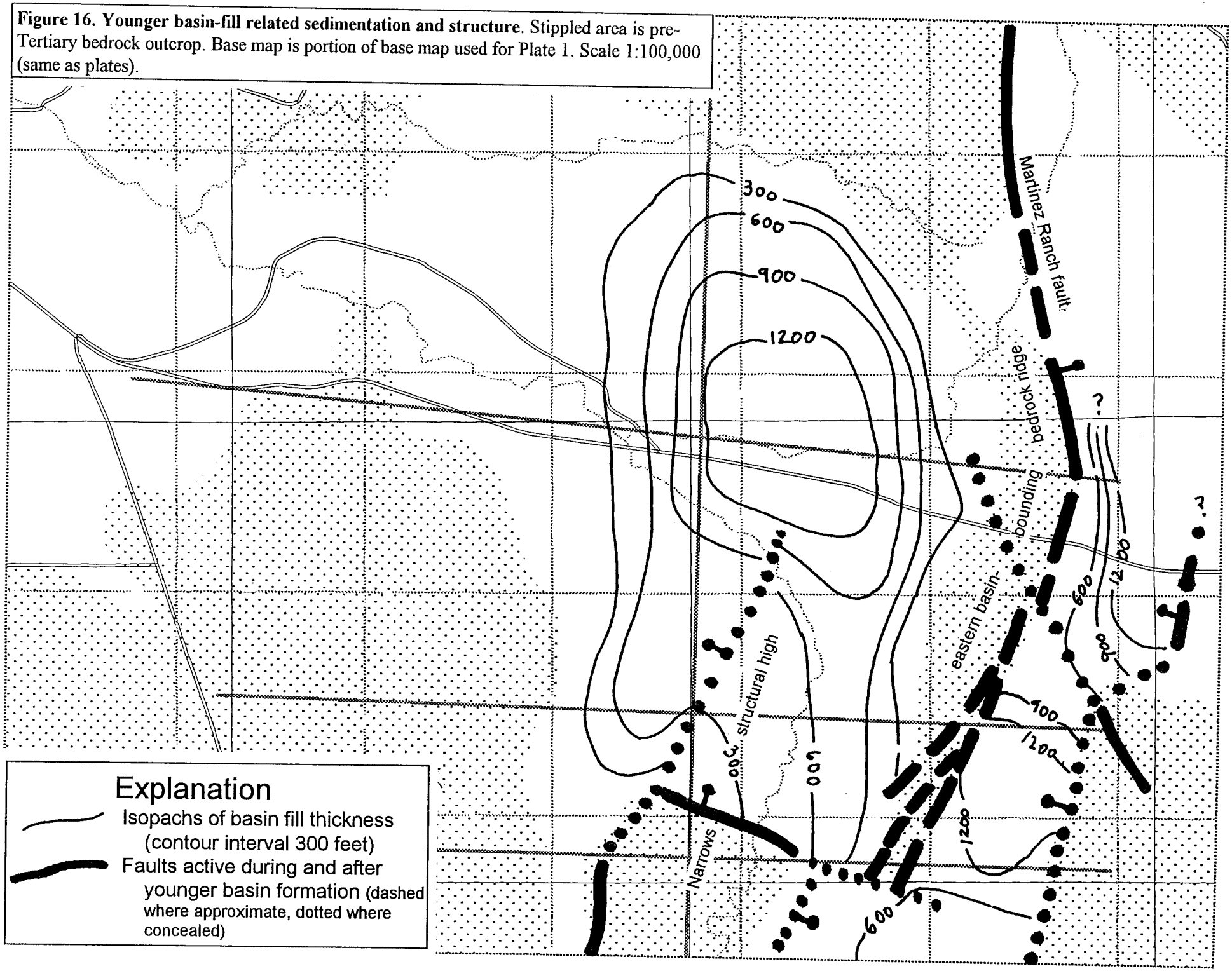

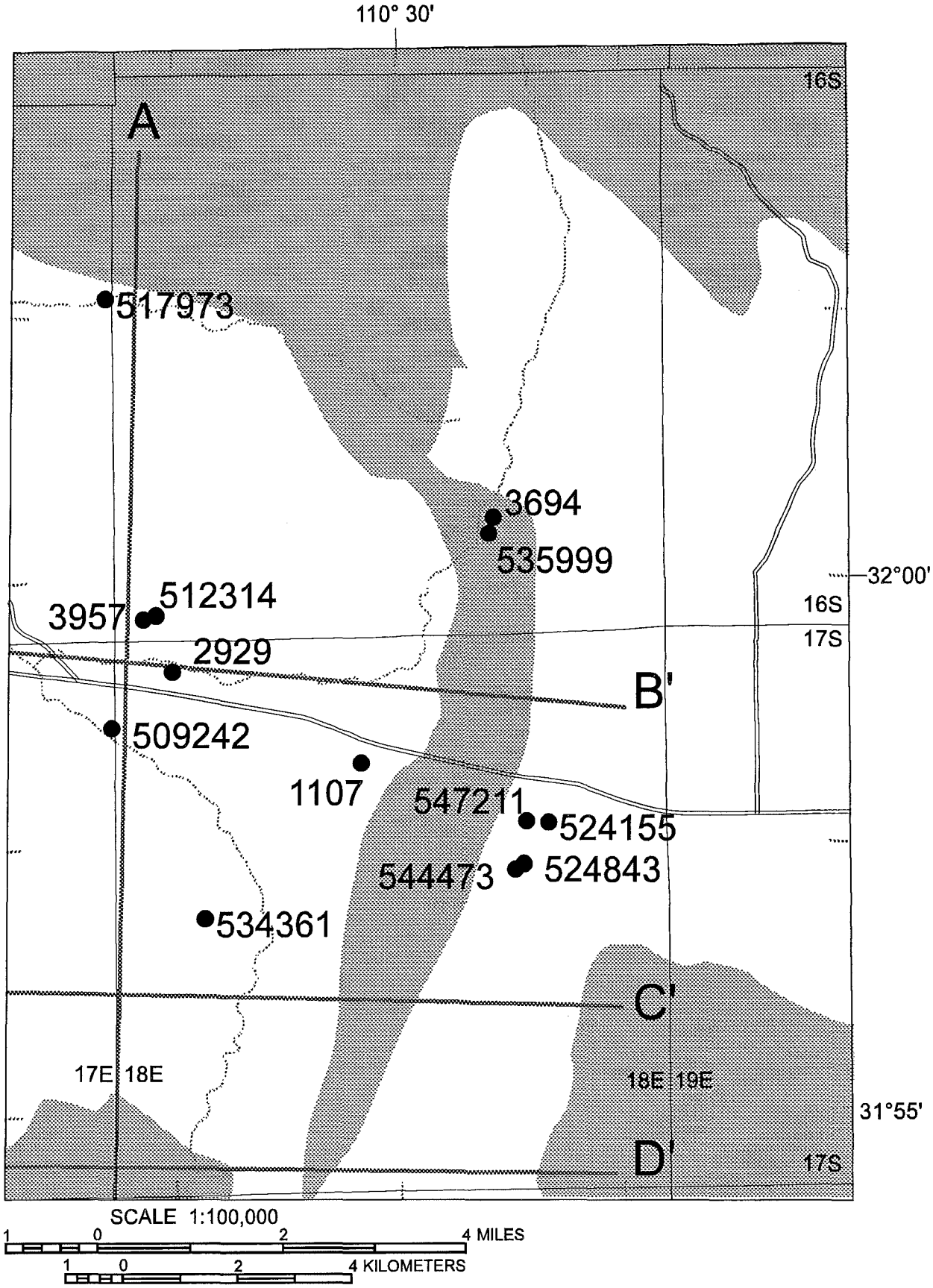

Figure 17. Locations of wells from which lithologic data was obtained for this study.

ID[1]	NAME	LOCATION	lithology major	tops, formations, rock types encountered	source of lithologic data[2]
1107	UNITED STATES ARMY #8B	D(17-18)9 ACC	silt, clay and sand, no gypsum; TD 580	0-200 silt to fine sand, tan, v. strong fizz, increasing sand at 170; minor quartzite and granite fragments present 200-290--no samples 290-390 silt to fine sand, tan, v. strong fizz 400-480 light gray clay to v. fine sand, v. strong fizz, possibly tuffaceous 490-580 grayish tan clay silt, v. strong fizz, no gypsum in any sample	cuttings logged by Ray Harris, 5/96
2929	ARIZONA STATE HIGHWAY DEPARTMENT	D(17-18)6 AC	silt fine sand, some tuffaceous(?); gypsum common; TD 900	10-80 sand to gravel (Qal?) 90-280 light brown sand, silt clay, with small fragments of secondary gypsum; moderate to strong fizz in much of the clay; decreasing sand with depth 290-430 no samples 440-550 medium brown clay, strong fizz 570-700 medium-light brown sand, silt-clay, and gypsum, calcite cement in sand 700 light gray tuff?, no fizz 720-730 moderately indurated silt, very fine sandstone fragments, gypsum, granite or gneiss fragments, weak or no fizz 740-800 medium brown moderately indurated clay silt-fragments, very abundant gypsum, minor tuff? fragments, no fizz 810-820 light brown silt, very fine sand, moderately indurated, moderate fizz, minor gypsum 830-840 light brown tuffaceous(?) silt to very fine sand, moderately indurated, abundant gypsum 850-900 medium to dark brown clay silt, some tuffaceous(?), minor gypsum, decreasing down hole, light brown indurated silt to fine tuffaceous(?) sand at bottom; strong fizz; induration increases down hole	cuttings logged by Ray Harris, 5/96
3694	JOHN RIBAR	D(16-18)26 CCA	brown clay, silt, fine sand; coarse sand to fine gravel ~125; TD 163	50-125 light gray-brown clay silt, coarsening down hole to mostly coarse sand to fine gravel 150 mostly dark brown clay-silt, minor coarse sand to fine gravel 163 dark brown silt to fine sand	cuttings logged by Ray Harris, 5/96
3957	E.T. BUD WALDEN	D(16-18)31 CCD	silt, fine sand; TD 730	20-730, medium brown clay-silt, slightly indurated, strong fizz 230-260, minor very fine sand 450-530 lighter brown, more silt 690-700 more silt 710-730 light brown to tan 730 some fine sand	cuttings logged by Ray Harris, 5/96
547211	John and Shannon Guilmartin	D(17-18)14BAA	contact 'fanluvial' to 'volcanics' (Kb?) at 250; TD 520	0-250 'fanluvial' 250-520 'volcanics'; probably Kb based on nearby outcrops, water from '1 foot gravel formation' at 470 feet, probably a fault zone?	Driller's report, interpreted by SMR 8/96

ID[1]	NAME	LOCATION	lithology major	tops, formations, rock types encountered	source of lithologic data[2]
524843	Roger Lance	D(17-18)14BDD	440-500 'clay'; 500-610 'shale-type rock'; TD 610	440-500 clay 500-610 shale-type rock	Driller's report, interpreted by SMR 8/96
524155	Jim Hunnicutt	D(17-18)14ABA	340-contact 'clay conglomerate' to 'conglomerate'; TD 460	0-20 dirt and clay 20-340 clay conglomerate 340-380 conglomerate 380 460 conglomerate, layers of rock	Driller's report, interpreted by SMR 8/96
534361	Irvin Blankenbaker	D(17-18)19AAA	480--contact 'clay' and 'clay conglomerate' to 'conglomerate'; TD 530	0-20 dirt and clay 20-260 clay 260-310 layer of sandstone 310-480 clay conglomerate 480-530 conglomerate (Titan Drilling Co.--seem to refer to hard rock as conglomerate?)	Driller's report, interpreted by SMR 8/96
544473	M.E. Wigen	D(17-18)14DAB	310--contact 'clay' to 'conglomerate'	0-20 dirt and clay 20-310 clay 310-380 conglomerate (Titan Drilling)	Driller's report, interpreted by SMR 8/96
509242	Empirita Ranch	D(17-17)1DDD	15-565--sand gravel, silt and clay; TD 565	0-15 sand, silt, gravel, cobbles and boulders (QTg??) 15-565 sand, gravel, silt and clay	Driller's report, interpreted by SMR 8/96
512314	E. T. Walden	D(16-18)31CAD	710-sandy clay with interbedded gypsum; 832-clayey sandstone; 850-cemented gravel and sand; 890-hard conglomerate, cemented sand (Kb???); TD 1010	0-710 unknown-reenter hole drilled 1979 by Frank Owenby 710-832 light brown to red sandy clay with interbedded gypsum 832-850 clayey sandstone 850-890 coarse gravel and sand, cemented 890-1010 hard conglomerate, cemented sand, gravel-cobbles (Bisbee???)	Driller's report, interpreted by SMR 8/96
535999	Dulonn L. Jefferson	D(16-18)26CCC	20--contact dirt and rock to rock (Kb?); TD 100	0-20 dirt and rock 20-100 rock (Kb? based on adjacent outcrops)	Driller's report, interpreted by SMR 8/96
517973	Charles J. Proctor	D(16-17)13ADA	400--contact 'clay and clay conglomerate' to 'rock'--probably detachment fault; TD 600	0-20 dirt and clay 20-400 clay and clay conglomerate (Titan Drilling Co. terminology) 400-600 rock (probably footwall of detachment fault)	Driller's report, interpreted by SMR 8/96

[1] four digit numbers are Arizona Geological Survey AzWell identifiers; 6 digit numbers are Arizona Department of Water resources well registration numbers.

[2] Cuttings logged by R.C. Harris are in the repository at the Arizona Geological Survey.

Middle Tertiary history

Middle Tertiary history is recorded by formation of the Pantano basin and subsequent dismemberment during a period of normal faulting in Early Miocene time. Sediments of the Pantano Formation are highly variable, ranging from strongly indurated conglomerate to poorly indurated mudstone. Lithology of conglomerate varies rapidly reflecting interfingering of alluvial fans draining mountains of Paleozoic and Mesozoic strata to the south and Paleozoic strata and crystalline rocks to the north. Data from wells drilled in the central basin indicates that gypsum is locally abundant there (Figure 17).

A zone of WNW-trending faults at the northern end of the Empire Mountains appears to be a dismembered fault system active during deposition of the Pantano Formation (Figure 15). In several places, stratigraphy in the Pantano Formation changes across these faults. The most obvious place is in the NE Empire Mountains (approx. 31°59'N, 110°35.5'W) where a WNW-trending fault that separates lower Pantano fanglomerate (Tpf) and Bisbee Group (Kb) dies out to the southeast and upper Pantano mudstone (Tpm) overlaps the fault to directly overly Bisbee Group. Interpretation of this fault system is based on integration of geologic mapping by Balcer [1984] and Finnell [1971]. A WNW-trending gravity gradient in the southern part of the lower Cienega Basin (Plate 2) may be a SE continuation of this zone.

Subsequent to deposition, the Pantano Formation was broken by a series of N to NNE-trending normal faults. Major faults of this system follow Davidson Canyon (Figure 15, Plate 1). Pantano Formation is faulted against Paleozoic strata (MYu) in the SW part of the map area. The dip of bedding in the Pantano Formation in the hanging wall of this fault is similar to that underlying Cretaceous volcanic rocks (Kv) and Bisbee Formation (Kb), suggesting that tilting of the northern Santa Rita block to the east may be due to Miocene normal faulting. This fault zone can be traced north and splits into three major splays traceable through the northern Empire Mountains to about Pantano Road (Figure 15, Plate 1). Between Pantano Road and Aqua Verde Creek these faults appear to merge into low-angle normal faults of the Catalina-Rincon detachment system in a zone of poorly exposed and structurally and stratigraphically complex Pantano Formation.

A NE-trending steep magnetic gradient crosses the central part of the Cienega basin. It is the major feature in the magnetic anomaly profile for section A-A' (Plate 3, 4). This gradient is interpreted to image a lateral ramp or tear fault in the Catalina-Rincon Detachment system. Unfractured crystalline rocks are closer to the surface (0 to 2 km) north of this zone than to the south (>4 km?). Rocks in the hanging wall of the detachment fault are expected to be highly faulted and fractured.

Upper Pantano Formation is mapped as mudstone in the outcrop area west of the Cienega Basin. Rock avalanche deposits (Tx) blanket this mudstone on an apparently nearly horizontal surface over about 9 km^2 in the area between Pantano Road and Aqua Verde Creek (approx. 32°02'N, 110°35'W). The base of these breccias maps out as a very gently dipping surface in spite of the highly variable strike and dip of underlying Pantano mudstone strata. The breccias have been mapped as the top of the Pantano Formation in this area [Balcer, 1984; Drewes, 1977], and interpreted to mark the onset of movement on the Catalina-Rincon detachment fault. The breccia units thin and pinch out just south of Interstate 10; the southernmost exposures are apparently concordant layers in an east-dipping section of mudstone and conglomerate. The dip of strata in this section decreases up section to the east into the flat-lying sandstone and conglomerate exposed at the surface in the central part of the Cienega Basin.

On the east side of the Cienega Basin, the basal tuff of the Pantano Formation is overlain by moderately to densely indurated, Bisbee-Group-clast conglomerate of the Pantano Formation. Quartzite breccia (derived from Kb?) capping ridges of Pantano conglomerate on the east side of the basin (31°57'N, 110°30'W) appear to be large slide blocks or rock avalanche deposits in the Pantano Formation section. Up section from the breccia the sediments fine continuously into weakly to moderately indurated sandy conglomerate and sandstone exposed in the bluffs along Cienega Creek.

This gradation allows for no clear distinction of Pantano Formation from overlying basin-fill sediment (QTg). Wells drilled in the central Cienega Basin penetrate 100's of feet of fine-grained sediment, locally containing gypsum, which is lithologically identical to Pantano mudstone. The dip of strata in these wells is unknown, so correlation of lithology with dip can be made, and again, there is no clear lithologic boundary between 'basin fill' (QTg) and Pantano mudstone (Tpm). The clear distinction of 'Nogales Formation' Paleozoic-clast conglomerate [Drewes, 1977; Balcer, 1984] above rock-avalanche and sedimentary breccia deposits, which can be made in the northwest part of the basin, disappears in the central and eastern part of the basin. The rocks cropping out in the southern part of the basin may be coeval with part of the Pantano mudstone (Tpm), the sedimentary breccia (Tx) and part of the Nogales Formation (QTg) in the northern part of the basin. Structural disruption related to the Catalina-Rincon detachment fault, and perhaps associated with emplacement of the rock avalanche deposits may have produced an angular unconformity that dies out at about the latitude of Interstate 10 into a concordant, and generally less disrupted, section.

The southern continuation of the Martinez Ranch fault, which bounds the eastern side of the high Rincon Mountains, can be traced along the east side of the bedrock high that bounds the Cienega Basin on the east (Figure 16). This fault apparently links with a series of northerly trending faults in the southeastern part of the basin in a right-stepping transfer zone. A belt of more steeply dipping strata, with dips of 20° as opposed to 5 to 10° is observed just west of Cienega Creek where it curves to a NW trend. This zone is interpreted to overlie the NNE continuation of the faults bounding the east side of the bedrock high that includes the Narrows on Cienega Creek. This fault appears to gain displacement to the south as the Martinez Ranch fault dies out. The Martinez Ranch fault and these northerly-trending faults that cut the youngest basin-filling sediment (QTg) are the youngest faults recognized in the study area.

The structure across the southern part of the Cienega basin is a gentle syncline with a diffuse hinge zone. This gentle syncline can be traced south of the basin, where the southeast-dipping Bisbee Group strata of the Empire Mountains form the west limb and the southwest-dipping Bisbee Group strata, and locally overlying Pantano-like sediments of the Whetstone Mountains, form the east limb. The Martinez Ranch fault and associated faults cut obliquely across this synform and are thus either coeval with the fold or younger.

COMPARISON WITH PREVIOUS MODEL

The basin thickness isopach map produced from this study (Figure 16) is broadly similar to the isopach map of basin thickness produced by Ellett [1994]. The 1200 foot contour encloses a larger area on the new map, and isopachs in the southern part of the basin are offset by a fault on the west side of the Narrows structural high. Also, the 1800-foot deep sub-basin inferred by Ellett [1994] on the west side of this structural high is not recognized. The basin area east of the eastern Cienega-basin-bounding bedrock ridge is depicted as a series of sub-basins, which are generally interpreted to be deeper on the new map than on Ellett's [1994] map. The gravity minimum in the central Cienega basin is not coincident with the deepest basin fill isopach because of the superimposed gravity anomalies from both the younger (QTg) and older (Tp) basin fill units. Interpretation of the structure on the base of the Pantano Formation is very sensitive to the poorly constrained and probably variable density contrast between the Pantano Formation and underlying rocks.

CONCLUSIONS

Geophysical data do not uniquely determine basin geometry, especially where the sub-basin geology is as complex as in the Cienega Basin area. A logical approach to the problem is to generate two bounding models—minimum and maximum likely thickness of basin fill. These could then be used as input for hydrologic models to see if they impact the results of these models. The maximum thickness model is deter-

mined by the minimum reasonable density contrast between low-density basin fill and underlying bedrock, and can be generated largely independent of the bedrock geology. The minimum thickness model is sensitive to how much of the gravity low over the basin is due to sub-basin geology, so a consideration of bedrock geology is more important. Removal of regional gravity gradients related to isostatic compensation for topography seems advisable to produce the most accurate results.

The revised model for the geometry of young basin fill in the lower Cienega basin is not significantly different from the existing model of Ellett [1994]. The inferred fault on the west side of the Narrows structural high (Figure 16) might impact the transmissivity of basin fill units along the fault. The new model for rock units underlying the low-density basin fill is significantly different. Fracture permeability is likely to be the major source of hydrologic transmissivity in these units, and the structural patterns depicted on Figures 15 and 16 should provide a framework for predicting orientation and density of fractures in these units.

Acknowledgments. Special thanks to Mark Gettings for providing digital gravity and areomagnetic data. Brenda Houser kindly provided unpublished field mapping by Tommy Finnell. Maurice Tatlow provided well driller reports for wells in the Cienega Basin area from Arizona Dept. of Water Resources files. Discussions with Brenda Houser, Mark Getting and Jon Spencer helped shape our interpretations. Use of software names does not constitute endorsement by Arizona Geological Survey.

REFERENCES

Aiken, C. L. V., 1976, The analysis of gravity anomalies of Arizona, Ph. D. dissertation: Tucson, Univ. Ariz., 127 p.

Andreasen, G. E., Mitchell, C. M., and Tyson, W. S., 1965, Aeromagnetic map of Tombstone and Vicinity, Cochise and Santa Cruz Counties, Arizona: U. S. Geological Survey Open-File Report 65-6, 1:125,000.

Balcer, Richard A., 1984, Stratigraphy and Depositional History of the Pantano Formation (Oligocene-Early Miocene), Pima County, Arizona, M. S. Thesis: Tucson, Univ. Ariz., 107 p.

Bankey, V. and Kleinkopf, M. D., 1985, Geophysical maps of the Whetstone Roadless Area, Cochise and Pima Counties, Arizona: U. S. Geological Survey Misc. Field Inv. Map 1614-C, 1:48000.

Bittson, A. G., 1976, Analysis of gravity data from the Cienega Creek area, Pima and Santa Cruz Counties, Arizona, M. S. Thesis: Tucson, Univ. Ariz., 76 p.

Dietz, D. D., 1985, Geophysical investigation of concealed bedrock pediments in central Avra Valley, Pima County, Arizona, M. S. Thesis: Tucson, Univ. Ariz., 75 p.

Drewes, H. D., 1974, Geologic map and sections of the Happy Valley quadrangle, Cochise County, Arizona: U. S. Geological Survey Map I-832, 1:48,000.

Drewes, H. D., 1977, Geologic Map and Sections of the Rincon Valley Quadrangle, Pima County, Arizona: U. S. Geological Survey Misc. Inv. Map MI-977, 1 sheet, 1:48000.

Drewes, H. D., 1981, Tectonics of southeastern Arizona, U. S. Geological Survey Professional Paper 1144, 96 p.

Ellett, William J., 1994, Geologic controls on the occurrence and movement of water in the lower Cienega Creek Basin, Tucson, Univ. Ariz., 116 p.

Finnell, T. L., 1971, Preliminary geologic map of the Empire Mountains quadrangle, Pima County, Arizona: U. S. Geological Survey Open-File Report.

Greenes, K. A., 1980, Application of the gravity method to groundwater volume determinations of alluvial basins, M. S. Thesis: Tucson, Univ. Ariz., 28 p.

Halvorson, P. H. F., 1984, An exploration gravity survey in the San Pedro Valley, southeastern Arizona, M. S. Thesis: Tucson, Univ. Ariz., 70 p.

Roudebush, Eric M., 1996, The influence of bedrock on perennial streamflow in the upper Cienega Creek Basin, Pima County, Arizona, MS thesis: Tucson, Univ. Ariz., 81 p.

Simpson, R.W., Jachens, R.C., Blakely, R.J., and Saltus, R.W., 1986, A new isostatic residual gravity map of the conterminous United States with a discussion on the significance of isostatic residual anomalies: Journal of Geophysical Research, v. 91, pp. 8248-8372.

Tucci, P., Schmocker, J. W., and Robbins, S. L., 1982, Borehole-gravity surveys in basin-fill deposits of central and southern Arizona, U. S. Geological Survey Open-File Report 82-473, 23 pages.

Webring, Michael, 1985, SAKI: A Fortran program for generalized linear inversion of gravity and magnetic profiles, U. S. Geological Survey Open-File Report 85-122, 29 pages.

APPENDIX 1: MODEL DESCRIPTIONS.

The following pages include table describing the geometric and geologic models used by SAKI for forward modeling of gravity and magnetic profiles. Each cross section is defined by two tables. The first is a list of the bodies in the cross section, with associated physical properties (density contrast and susceptibility), and a list of vertices defining the outline of the body. The second table lists the X,Z coordinates of the vertices. These tables have been edited for human readability from the SAKI model files.

Section A-A', Vertices

vertex #	X	Z	vertex #	X	Z	vertex #	X	Z
1	-60.96	-1.219	37	4.968	0.914	73	6.38	-1.11
2	-0.244	-1.219	38	5.3	2	74	7.84	-0.88
3	0	-1.311	39	4.572	6	75	9.327	-0.78
4	0.213	-1.244	40	2.896	8	76	10.302	-0.68
5	0.488	-1.244	41	1.859	10	77	11.552	-0.66
6	0.671	-1.295	42	6	2.25	78	12.131	1.4
7	-0.305	-0.61	43	6.706	10.1	79	9.51	0.732
8	-1.585	0.366	44	3.048	10.1	80	7.559	0.427
9	-3.2	1.524	45	4.694	-1.18	81	9.357	8.178
10	-5.182	10.1	46	5.212	-1.15	82	13.823	-0.58
11	-60.96	10.1	47	5.578	-1.19	83	13.076	-0.6
12	0.823	-1.311	48	5.624	-1.15	84	12.436	-0.518
13	1.006	-1.28	49	5.944	0.152	85	13.594	0.6
14	1.402	-0.152	50	6.066	0.518	86	15.941	-0.686
15	1.798	9.964	51	5.395	0.488	87	15.606	-0.716
16	0.274	10	52	4.176	-1.295	88	15.149	-0.762
17	-1.219	9.936	53	4.633	-1.219	89	15.758	-0.265
18	-2.438	10.1	54	6.523	-1.219	90	18.364	-1.158
19	1.219	-1.234	55	10.058	-1.097	91	18.582	-1.105
20	1.341	-1.244	56	10.455	-1.128	92	17.748	-0.933
21	1.89	-1.259	57	12.07	-1.119	93	16.5	-1
22	2.225	-1.25	58	16.855	-1.219	94	19.385	-1.158
23	2.454	-1.286	59	17.16	-1.158	95	19.964	-1.341
24	2.743	-1.256	60	17.496	-1.158	96	20.163	-1.311
25	2.896	-1.28	61	16.794	-1.097	97	20.391	-1.356
26	3.048	-1.25	62	16.093	-1.006	98	20.513	-1.326
27	3.2	-1.25	63	15.484	-0.945	99	100	-1.341
28	3.536	-1.311	64	14.661	-0.838	100	100	10.1
29	3.84	-1.28	65	13.99	-0.762	101	20.574	10.1
30	3.962	-1.286	66	13.35	-0.701	102	1.341	-1.006
31	3.993	-1.28	67	12.619	-0.686	103	1.067	-1.097
32	4.68	0.28	68	11.643	-0.686	104	7.315	2.45
33	3.962	0.2	69	10.546	-0.701	105	28	-2.74
34	2.195	0.2	70	9.388	-0.82	106	38	-2.74
35	1.366	-0.5	71	7.85	-0.97	107	48	-1.4
36	4.724	0.335	72	6.4	-1.13			

Section A-A', Body specifications

rock unit	body number	density contrast	susceptibility	prism front	prism back	vertices
bisbee	1	-0.077	0	20	-20	1 2 3 4 5 6 7 8 9 10 11
paleozoic	2	-0.012	0	20	-20	6 12 13 103 14 15 16 17 18 10 9 8 7
precambrian	3	-0.02	5.37E-03	20	-20	15 41 40 39 38 42 43 44 18 17 16
bisbee	4	-0.05	0	20	-20	13 19 20 102 103
paleozoic	5	-0.07	0	20	-20	103 102 35 14
bisbee	6	-0.05	0	20	-20	20 21 22 23 24 25 26 27 28 29 30 31 32 33 34 35 102
paleozoic	7	0	0	20	-20	35 34 33 32 36 37 38 39 40 41 15 14
nogales	8	-0.5	0	20	-20	30 52 53 54 55 56 57 58 59 60 61 62 63 64 65 66 67 68 69 70 71 72 47 46 45 31
bisbee	9	-0.05	0	20	-20	31 45 46 47 48 49 50 51 36 32
body 10	10	-0.3	0	20	-20	47 72 71 70 69 68 77 76 75 74 73 48
bisbee	11	-0.05	0	20	-20	48 73 74 75 76 77 68 84 83 82 85 78 79 80 49
paleozoic	12	0.02	0	20	-20	49 80 79 78 81 104 42 38 37 36 51 50
precambrian	13	-0.02	0	20	-20	42 104 81 43
	14	-0.3	0	20	-20	68 67 66 65 82 83 84
pantano	15	-0.3	0	20	-20	64 63 62 86 87 88
bisbee	16	-0.05	0	20	-20	65 64 88 87 86 89 85 82
pantano	17	-0.45	0	20	-20	62 61 60 90 91 92 93
bisbee	18	-0.07	0	20	-20	62 93 92 89 86
body19	19	-0.02	2.19E-03	20	-20	90 94 95 96 97 98 101 43 81 78 85 89 92 91
body 20	20	-0.015	3.00E-03	20	-20	98 105 106 107 99 100 101

Section B-B', Vertices

Vertex ID	X	Z	Vertex ID	X	Z	Vertex ID	X	Z
1	-100	-1.067	20	4.4	-0.98	39	7.291	-3
2	-0.884	-1.067	21	4.023	-1	40	7.513	-3
3	0.0	-1.079	22	3.53	-1	41	7.559	-3
4	-0.2	-1	23	2.896	-0.914	42	7.538	-3
5	0.2	-1.097	24	2.621	-0.975	43	8.062	-3
6	1.341	-1.097	25	2.286	-0.97	44	8.077	-1.097
7	1.57	-1.122	26	1.949	-0.981	45	8.153	-3
8	1.829	-1.103	27	1.499	-0.768	46	8.138	-3
9	2.012	-1.128	28	3.1	0.15	47	8.321	-3
10	2.195	-1.097	29	0.2	0.1	48	8.336	-1.094
11	2.408	-1.091	30	1.1	1.05	49	8.37	-0.908
12	2.652	-1.067	31	5.547	-1.097	50	8.626	-3
13	2.728	-1.064	32	5.675	-1.097	51	8.55	-1.082
14	3.078	-1.058	33	6.157	-1.091	52	8.611	-1.097
15	3.2	-1.097	34	6.675	-1.103	53	9.464	-1.097
16	3.331	-1.097	35	6.895	-1.122	54	9.6	-0.956
17	4.115	-1.097	36	7.26	-1.097	55	9.7	-0.97
18	4.206	-1.088	37	7.269	-3	56	10.7	0.9
19	4.548	-1.097	38	7.279	-3	57	10.48	1.3

Vertex ID	X	Z
58	10.3	1.3
59	8.412	-0.79
60	7.696	-1
61	7.65	-0.97
62	7.254	-1
63	6.645	-1.05
64	5.974	-0.96
65	5.959	-0.95
66	5.928	-0.92
67	5.204	1
68	5.258	1
69	5.883	1.2
70	6.248	1.2
71	6.9	1.2
72	7.55	0.328
73	8.5	0.6
74	8.7	0.7
75	9.921	-1.082
76	9.967	-1.073
77	10.257	-1.073
78	10.272	-1.085
79	12.619	-1.103
80	12.78	-1.122
81	13.106	-1.113
82	15.545	-1.177
83	16.825	-1.152
84	18.044	-1.189
85	17.6	-1.021
86	17.587	-3
87	17.5	-1
88	16.093	-1
89	14.722	-1.162
90	15.088	-1
91	14.874	-1
92	13.5	-1
93	13.411	-1.013
94	10	-0.852
95	9.6	-0.87
96	11	-0.8
97	13.472	-0.646
98	14.585	-3
99	14.722	-3
100	13.49	-0.9
101	16.886	-3
102	16.478	-0.6
103	17.2	-0.65
104	19.69	-1.219
105	19.721	-1.097
106	20.818	-0.6
107	21.671	-0.16
108	22.555	0.3
109	22.555	-0.3
110	21.915	-0.6
111	21.123	-1.05
112	20.604	-1.25
113	20.757	-1.244
114	22.555	-1.274
115	100	-1.28
116	100	1.463
117	100	10
118	22.555	10
119	22.555	1.463
120	21.704	0.704
121	20.253	0.603
122	19.5	3.5
123	16.916	3.5
124	15	0.89
125	14.112	0.9
126	12.2	1
127	7	1.3
128	7.8	1.5
129	1.707	10
130	2.134	1.754
131	0.975	10
132	-100	10
133	-100	2.407
134	20.315	-1.227
135	-100	0.947
136	12.2	10
137	7.8	10
138	9.55	-0.599
139	7.529	0.325
140	4.037	-0.63
141	16.989	0.573
142	16.5	0.88
143	-0.49	-0.1
144	-100	0.5
145	-5.4	-1.067
146	-6	0
147	-6.5	0.6

Section B-B', Body specifications

rock unit	body #	density contrast	susc	prism front	prism back	vertices
bisbee	1	-0.018	0	20	-20	145 2 4 3 5 27 26 25 24 12 13 23 14 15 16 22 21 20 140 28 29 143 146
pantano	2	-0.3	0	1	-4	2 3 4
pantano	3	-0.25	0	1	-4	5 6 7 8 9 10 11 24 25 26 27
alluvium	4	-0.3	0	1	-4	11 12 24
pantano	5	-0.3	0	0.1	-20	13 14 23
pantano	6	-0.25	0	0.1	-20	16 17 18 21 22
pantano	7	-0.25	0	0.2	-20	18 19 20 21
bisbee	8	-0.002	0	20	-20	19 31 66 65 64 63 62 61 60 59 138 56 74 73 72 139 140 20
bisbee	9	-0.01	0	20	-20	95 94 96 97 100 102 103 87 85 84 104 105 106 107 108 119 120 121 141 142 124 125 126 56 138
rhyolite	10	-0.02	8.00E-03	0	-20	31 32 65 66
pantano	11	-0.3	0	0	-20	32 33 64 65

rock unit	body #	density contrast	susc	prism front	prism back	vertices
pantano	12	-0.3	0	0.1	-20	33 34 35 36 44 48 49 59 60 61 62 63 64
nogales	13	-0.5	0	3.5	-5	53 75 76 77 78 79 80 81 89 82 83 84 85 87 88 90 91 92 93 55 54
pantano	14	-0.3	0	20	-20	94 95 55 93 92 100 97 96
pantano	15	-0.3	0	20	-20	90 88 87 103 102 100 92 91
volc sediment	16	-0.25	0	20	-20	104 134 111 110 109 108 107 106 105
basin fill	17	-0.45	0	20	-20	134 112 113 114 109 110 111
bisbee	18	-0.05	0	20	-20	114 115 116 119 108 109
lower plate	19	-0.05	1.28E-04	20	-20	119 116 117 118
lower plate	20	-0.056	3.21E-03	20	-20	128 57 126 136 137
bisbee	21	0.05	2.20E-03	20	-20	28 67 68 69 70 71 139 72 73 74 56 57 58 127 30 143 29
precambrian	22	-0.05	2.00E-03	20	-20	135 147 30 127 58 57 128 130 133
new lower plate	23	-0.06	2.26E-03	20	-20	126 125 124 123 122 120 119 118 136
left lower plate	24	-0.024	1.27E-03	20	-20	128 137 129 131 132 133 130
right yg	25	0.05	2.20E-03	20	-20	126 57 56
pantano	26	-0.3	0	20	-20	48 51 52 53 54 55 95 138 59 49
Paleozoic	27	0.11	0	20	-20	140 139 71 70 69 68 67 28
paleozoic	28	0.04	0	5	-20	124 142 120 122 123
paleozoic	29	0.11	0	20	-20	143 30 147 146
paleozoic	30	0.04	0	5	-20	142 141 121 120
Tucson Basin	31	-0.4	0	20	-12	1 145 146 147 135 144

Section C-C', Gravity model, Vertices

vertex #	X	Z	vertex #	X	Z	vertex #	X	Z
1	-15.24	-1.219	18	-0.213	-0.3	35	1.707	-1.234
2	-0.396	-1.219	19	-0.488	-0.5	36	2.103	-1.113
3	-0.671	-0.771	20	0.838	-1.082	37	2.49	-0.991
4	-1.128	-0.5	21	0.869	-1.036	38	2.316	-0.61
5	-1.89	1.661	22	0.777	-0.762	39	2.073	-0.091
6	-2.697	10	23	1.036	-0.625	40	1.981	-1.311
7	-15.24	10	24	1.615	0.183	41	2.042	-1.372
8	0.725	-1.143	25	1.829	0.335	42	2.316	-1.301
9	0.939	-1.158	26	1.646	1.1	43	2.53	-1.286
10	0.631	-1.067	27	0.7	1.2	44	2.621	-1.298
11	0.198	-0.945	28	0.7	-0.168	45	2.6	-1.244
12	-0.213	-0.838	29	0.732	-0.64	46	2.3	-1.259
13	0.664	-0.914	30	-1.158	1	47	2.56	-1.143
14	0.695	-0.762	31	-1	1.646	48	2.53	-1.106
15	0.427	-0.3	32	-1	2.316	49	2.652	-1.036
16	0.259	-0.1	33	-1	10	50	2.5	-0.64
17	0.061	-0.1	34	1.097	-1.158	51	2.5	-0.152

vertex #	X	Z
52	2.5	0.488
53	2.3	3
54	0	10
55	2.859	-1.244
56	3.109	-1.13
57	3.383	-0.92
58	3.353	-0.64
59	3.322	-0.549
60	2.926	-0.875
61	2.957	-1.219
62	3.408	-1.225
63	3.399	-1.128
64	3.901	-1.228
65	4.13	-1.25
66	4.13	-0.88
67	3.932	-1.02
68	3.688	-1.067
69	4.13	-0.579
70	3.749	-0.61
71	4.267	-1.265
72	4.45	-1.372
73	4.663	-1.28
74	5.7	-0.5
75	6.553	0.15
76	7.54	0.9
77	8.2	1.3
78	7.2	1.92
79	0.5	10
80	6.3	1.38
81	5.9	0.9
82	4.907	0.2
83	4.724	-1.265
84	4.831	-1.241
85	5.029	-1.25
86	5.77	-1.25
87	5.883	-1.228
88	6.066	-1.241
89	6.614	-1.204
90	7.209	-1.2
91	7.65	-1.16
92	8.108	-0.671
93	8.565	-0.39
94	9.022	-0.39
95	9.6	-0.2
96	9.37	0.305
97	9.266	0.488
98	8.6	0.88
99	8.2	0.47
100	7.45	-0.2
101	6.523	-0.671
102	6.675	-1.225
103	8.199	-1.219
104	8.489	-1.183
105	8.626	-1.242
106	9.815	-1.219
107	10.241	-1.17

vertex #	X	Z
108	10.851	-1.219
109	11.46	-1.219
110	11.595	-1.164
111	12.192	-1.164
112	12.436	-1.204
113	13.259	-1.219
114	13.716	-1.219
115	13.838	-1.244
116	14.006	-1.219
117	14.112	-1.219
118	14.225	-1.128
119	13.838	-0.936
120	13.472	-0.75
121	12.9	-0.58
122	12	-0.95
123	11.339	-1.1
124	10.698	-1.1
125	10.241	-1.14
126	10.15	-1.14
127	9.967	-1.16
128	9.952	-1.15
129	9	-1.14
130	8.5	-1
131	8.2	-1.1
132	11.278	-0.533
133	11.049	-0.122
134	10.516	0.213
135	9.906	0.396
136	9.906	-0.5
137	11.2	-1
138	9.693	-0.396
139	11.201	-1.145
140	12.101	-1.16
141	12.741	-1.15
142	14	-1.113
143	14.28	-1.067
144	14.368	-1.219
145	15.261	-1.219
146	15.514	-1.25
147	15.712	-1.289
148	15.911	-1.28
149	16.087	-1.311
150	16.292	-1.295
151	16.511	-1.286
152	16.968	-1.323
153	17.831	-1.326
154	18.084	-1.311
155	18.044	-1.219
156	18.014	-1.18
157	17.252	-1.082
158	16.353	-0.9
159	15.758	-0.97
160	15.712	-1.01
161	15.575	-1.05
162	13.625	-0.7
163	13.89	-0.63

vertex #	X	Z
164	13.89	-0.43
165	14.082	-0.2
166	14.143	-0.27
167	14.341	-0.07
168	14.417	-0.12
169	15.4	0.1
170	16.2	0.3
171	16.2	1.158
172	16	3
173	16	10
174	18.379	-1.332
175	18.379	-1.19
176	18.379	-1.12
177	18.379	10
178	18.776	-1.2
179	19.446	-1.335
180	21.336	-1.341
181	45.72	-1.341
182	45.72	10
183	21.336	10
184	21.336	-0.7
185	20.33	-0.6
186	19.172	-0.8

Section C-C', Gravity model, Body specifications

body #	unit	density contrast	susc	prism front	prism back	vertices
1	bisbee	-0.045	0	20	-20	1 2 3 4 5 6 7
2	bisbee	-0.05	0	20	-20	2 8 9 10 11 12 3
3	Paleozoic	0.04	0	20	-20	3 12 11 10 13 14 15 16 17 18 19 4
4	empire stock	-0.031	3.41E-03	20	-20	4 19 18 17 16 15 14 29 28 27 26 25 39 51 52 53 54 33 32 31 30 5
5	bisbee	-0.05	0	20	-20	5 30 31 32 33 6
6	paleozoic	0.04	0	20	-20	10 9 34 35 36 37 38 39 25 24 23 22 21 20 13
7	empire stock	-0.01	1.00E-03	20	-20	13 20 21 22 29 14
8	precambrian	-0.05	1.50E-03	20	-20	22 23 24 25 26 27 28 29
9	glance	0.02	0	20	-20	40 41 42 43 44 45 46
10	gardner	-0.02	0	20	-20	40 46 47 48 37 36 35
11	glance	0.02	0	20	-20	55 61 62 63 57 56
12	paleozoic	0.04	0	20	-20	44 55 56 57 58 59 60 47 45
13	glance	0.02	0	20	-20	62 64 65 66 67 68 63
14	paleozoic	0.04	0	20	-20	63 68 67 66 69 70 58 57
15	precambrian	-0.017	1.41E-03	20	-20	47 60 59 58 70 82 81 80 78 79 54 53 52 51 50 49 48
16	paleozoic	0.061	0	20	-20	65 71 72 73 74 75 76 77 78 80 81 82 70 69 66
17	glance	0	0	20	-20	73 83 84 85 86 87 101 100 99 98 77 76 75 74
18	bisbee	-0.045	0	20	-20	87 88 89 90 91 92 93 94 95 96 97 98 99 100 101
19	pantano	-0.05	0	20	-20	91 131 130 129 128 138 95 94 93 92
20	nogales	-0.5	0	20	-20	89 102 103 104 105 106 107 108 109 110 111 112 113 114 115 116 142 141 140 139 125 126 127 128 129 130 131 91 90
21	bisbee	-0.045	0	20	-20	128 127 126 125 124 123 132 133 137 136 96 95 138
22	glance	0.041	0	20	-20	96 136 137 133 134 135 97
23	pantano	-0.3	0	20	-20	125 139 140 141 142 116 117 118 119 120 121 122 123 124
24	paleozoic	0.03	0	3	0.7	123 122 121 120 162 163 164 165 166 167 168 169 170 171 172 78 77 98 97 135 134 133 132
25	pantano	-0.5	0	20	-20	117 144 143 118
26	precambrian	-0.08	1.97E-03	20	-20	144 145 146 161 160 159 158 157 156 155 175 176 186 185 184 183 177 173 172 171 170 169 168 167 166 165 164 163 162 120 119 118 143
27	alluvium	-0.35	0	20	-20	146 147 148 149 150 151 152 153 154 155 156 157 158 159 160 161
28	alluvium	-0.35	0	20	-20	154 174 179 178 175 155
29	bisbee	-0.06	0	20	-20	175 178 179 180 184 185 186 176
30	precambrian	-0.028	2.51E-03	20	-20	180 181 182 183 184
31	precambrian	-0.039	4.17E-03	20	-20	78 172 173 79
32	paleozoic	0.04	0	20	-20	48 49 50 51 39 38 37

Section C-C', Magnetic model, Vertices

Vertex #	X	Z	Vertex #	X	Z	Vertex #	X	Z
1	-15.24	-1.219	60	2.926	-0.875	119	13.838	-0.936
2	-0.396	-1.219	61	2.957	-1.219	120	13.472	-0.792
3	-0.671	-0.771	62	3.408	-1.225	121	12.68	-0.686
4	-1.128	-0.6	63	3.399	-1.128	122	12.222	-0.701
5	-1.89	1.661	64	3.901	-1.228	123	11.339	-0.823
6	-2.697	10	65	4.13	-1.25	124	10.698	-0.96
7	-15.24	10	66	4.13	-0.823	125	10.241	-1.097
8	0.725	-1.143	67	3.932	-0.975	126	10.15	-1.097
9	0.939	-1.158	68	3.688	-1.067	127	9.967	-1.067
10	0.631	-1.067	69	4.13	-0.579	128	9.952	-1.006
11	0.198	-0.945	70	3.749	-0.61	129	9.671	-0.884
12	-0.213	-0.838	71	4.267	-1.265	130	8.9	-0.896
13	0.664	-0.914	72	4.45	-1.372	131	8.352	-0.957
14	0.695	-0.762	73	4.663	-1.28	132	11.278	-0.533
15	0.427	-0.3	74	5.7	-0.6	133	11.049	-0.122
16	0.259	-0.1	75	6.553	0.15	134	10.516	0.213
17	0.061	-0.2	76	7.742	0.6	135	9.906	0.396
18	-0.213	-0.2	77	8.4	1	136	9.906	0.244
19	-0.488	-0.75	78	7.2	1.92	137	10.546	0.116
20	0.838	-1.082	79	0.5	10	138	9.693	-0.396
21	0.869	-1.036	80	6.3	1.38	139	11.201	-1.097
22	0.777	-0.762	81	5.9	0.9	140	12.101	-1.097
23	1.036	-0.625	82	4.907	0.2	141	12.741	-1.103
24	1.615	0.183	83	4.724	-1.265	142	13.646	-1.113
25	1.829	0.335	84	4.831	-1.241	143	14.28	-1.067
26	1.646	1.1	85	5.029	-1.25	144	14.368	-1.219
27	0.7	1.2	86	5.77	-1.25	145	15.261	-1.219
28	0.7	-0.168	87	5.883	-1.228	146	15.514	-1.25
29	0.732	-0.64	88	6.066	-1.241	147	15.712	-1.289
30	-1.158	1	89	6.614	-1.204	148	15.911	-1.28
31	-1	1.646	90	7.209	-1.067	149	16.087	-1.311
32	-1	2.316	91	7.65	-1.021	150	16.292	-1.295
33	-1	10	92	8.108	-0.671	151	16.511	-1.286
34	1.097	-1.158	93	8.565	-0.305	152	16.968	-1.323
35	1.707	-1.234	94	9.022	0.003	153	17.831	-1.326
36	2.103	-1.113	95	9.388	0.265	154	18.084	-1.311
37	2.49	-0.991	96	9.37	0.305	155	18.044	-1.219
38	2.316	-0.61	97	9.266	0.488	156	18.014	-1.18
39	2.073	-0.091	98	8.6	0.88	157	17.252	-1.082
40	1.981	-1.311	99	8.2	0.47	158	16.353	-1.05
41	2.042	-1.372	100	7.45	-0.2	159	15.758	-0.875
42	2.316	-1.301	101	6.523	-0.671	160	15.712	-0.98
43	2.53	-1.286	102	6.675	-1.225	161	15.575	-1.05
44	2.621	-1.298	103	8.199	-1.219	162	13.625	-0.8
45	2.6	-1.244	104	8.489	-1.183	163	13.89	-0.73
46	2.3	-1.259	105	8.626	-1.242	164	13.89	-0.53
47	2.56	-1.143	106	9.815	-1.219	165	14.082	-0.66
48	2.53	-1.106	107	10.241	-1.17	166	14.143	-0.77
49	2.652	-1.036	108	10.851	-1.219	167	14.341	-0.73
50	2.5	-0.64	109	11.46	-1.219	168	14.417	-0.9
51	2.5	-0.152	110	11.595	-1.164	169	15.088	-1.1
52	2.5	0.488	111	12.192	-1.164	170	16.5	0.183
53	2.3	3	112	12.436	-1.204	171	16.7	1.158
54	0	10	113	13.259	-1.219	172	17.8	3
55	2.859	-1.244	114	13.716	-1.219	173	16	10
56	3.109	-1.036	115	13.838	-1.244	174	18.379	-1.332
57	3.383	-0.823	116	14.006	-1.219	175	18.379	-1.22
58	3.353	-0.64	117	14.112	-1.219	176	18.379	-1.12
59	3.322	-0.549	118	14.225	-1.128	177	18.379	10

Vertex #	X	Z
178	18.776	-1.259
179	19.446	-1.335
180	21.336	-1.341
181	45.72	-1.341
182	45.72	10
183	21.336	10
184	21.336	-0.7
185	20.33	-0.6
186	19.172	-0.8

Section C-C', Magnetic model, Body specifications

body #	unit	density contrast	susc	prism front	prism back	vertices
1	bisbee	-0.02	0	20	-20	1 2 3 4 5 6 7
2	bisbee	-0.02	0	20	-20	2 8 9 10 11 12 3
3	paleozoic	0.04	0	20	-20	3 12 11 10 13 14 15 16 17 18 19 4
4	empire stock	-0.01	3.41E-03	20	-20	4 19 18 17 16 15 14 29 28 27 26 25 39 51 52 53 54 33 32 31 30 5
5	bisbee	0.02	0	20	-20	5 30 31 32 33 6
6	paleozoic	0.04	0	20	-20	10 9 34 35 36 37 38 39 25 24 23 22 21 20 13
7	empire stock	-0.01	1.00E-03	20	-20	13 20 21 22 29 14
8	precambrian	-0.02	1.50E-03	20	-20	22 23 24 25 26 27 28 29
9	glance	0.02	0	20	-20	40 41 42 43 44 45 46
10	gardner	-0.02	0	20	-20	40 46 47 48 37 36 35
11	glance	0.02	0	20	-20	55 61 62 63 57 56
12	paleozoic	0.04	0	20	-20	44 55 56 57 58 59 60 47 45
13	glance	0.02	0	20	-20	62 64 65 66 67 68 63
14	paleozoic	0.04	0	20	-20	63 68 67 66 69 70 58 57
15	precambrian	-0.02	1.41E-03	20	-20	47 60 59 58 70 82 81 80 78 79 54 53 52 51 50 49 48
16	paleozoic	0.04	0	20	-20	65 71 72 73 74 75 76 77 78 80 81 82 70 69 66
17	glance	0.02	0	20	-20	73 83 84 85 86 87 101 100 99 98 77 76 75 74
18	bisbee	-0.02	0	20	-20	87 88 89 90 91 92 93 94 95 96 97 98 99 100 101
19	pantano	-0.3	0	20	-20	91 131 130 129 128 138 95 94 93 92
20	nogales	-0.5	0	20	-20	89 102 103 104 105 106 107 108 109 110 111 112 113 114 115 116 142 141 140 139 125 126 127 128 129 130 131 91 90
21	bisbee	-0.02	0	20	-20	128 127 126 125 124 123 132 133 137 136 96 95 138
22	glance	0.02	0	20	-20	96 136 137 133 134 135 97
23	pantano	-0.3	0	20	-20	125 139 140 141 142 116 117 118 119 120 121 122 123 124
24	precambrian	0.04	1.18E-03	-0.9	-4	123 122 121 120 162 163 164 165 166 167 168 169 170 171 172 78 77 98 97 135 134 133 132
25	pantano	-0.3	0	20	-20	117 144 143 118
26	precambrian	-0.02	1.97E-03	20	-20	144 145 146 161 160 159 158 157 156 155 175 176 186 185 184 183 177 173 172 171 170 169 168 167 166 165 164 163 162 120 119 118 143
27	alluvium	-0.5	0	20	-20	146 147 148 149 150 151 152 153 154 155 156 157 158 159 160 161
28	alluvium	-0.5	0	20	-20	154 174 179 178 175 155
29	bisbee	-0.02	0	20	-20	175 178 179 180 184 185 186 176
30	precambrian	-0.02	2.51E-03	20	-20	180 181 182 183 184
31	precambrian	-0.02	4.17E-03	20	-20	78 172 173 79
32	paleozoic	0.04	0	20	-20	48 49 50 51 39 38 37

Section D-D', Vertices

vertex #	X	Z
1	0	-1.219
2	1.219	-1.25
3	1.463	-1.295
4	1.707	-1.265
5	1.298	-0.717
6	0.957	-0.914
7	3.368	-1.353
8	3.688	-1.402
9	3.993	-1.585
10	4.282	-1.585
11	4.526	-1.463
12	4.35	-1.35
13	4.938	-1.372
14	5.334	-1.402
15	5.334	-1.28
16	5.395	-1.189
17	6	-1.158
18	6.248	-1.311
19	6.401	-1.341
20	6.828	-1.356
21	7.041	-1.372
22	7.894	-1.311
23	7.864	-1.28
24	7.772	-0.914
25	7.498	-0.47
26	7.5	1.2
27	6.949	1.55
28	6.746	1.466
29	2.9	1.2
30	3.397	-0.491
31	4.33	-1.34
32	8.382	-1.341
33	11.217	-1.189
34	12.055	-1.25
35	12.16	-1.07
36	12.3	-0.9
37	11.644	-0.562
38	11.2	-1.13
39	9.8	-0.55
40	13.2	0.061
41	12.594	0.4
42	12.589	0.464
43	12.2	1.006
44	11.521	1.391
45	10.577	1.524
46	8.534	1.235
47	13.807	-1.265
48	13.62	-1.1
49	13.259	-1
50	13.929	-1.288
51	14.295	-1.25
52	14.42	-1.17
53	14.417	-0.945
54	13.914	0.5
55	14.9	-1.18
56	14.95	-0.35
57	14.493	-1.295
58	15.331	-1.326
59	15.575	-1.28
60	16.093	-1.341
61	16.84	-1.301
62	17.68	-1.3
63	17.65	-1.15
64	17.62	-1
65	16.307	-1.05
66	16.09	-0.95
67	17	-0.05
68	16.2	-0.335
69	16.093	0.122
70	14.387	1.341
71	13	2.225
72	19.1	-1.356
73	18.079	0.5
74	15.773	1.7
75	18.654	4.048
76	12	4.048
77	11.704	4.048
78	1.186	4.048
79	-5	3.048
80	-10	3.048
81	-10	-1.22
82	100	-1.22
83	100	4.048
84	-0.886	0
85	-3.765	2
86	2.7	1.2
87	2	1.2
88	1.682	0.239
89	1.5	-1.091
90	1.845	1.405
91	-2.783	1.039
92	3.1	-0.48

Section D-D', Body specifications,

body #	unit	density contrast	susc	prism front	prism rear	vertices
1	granite	-0.007	2.93E-03	20	-20	1 2 6 5 88 84
2	paleozoic	0.013	0	20	-20	2 3 4 89 5 6
3	paleozoic	0.013	0	20	-20	7 8 9 10 11 12 31
4	glance	-0.05	0	20	-20	11 13 15 17 16 12
5	bisbee	-0.021	0	20	-20	13 14 18 19 20 23 24 25 17 15
6	alluvium	-0.3	0	20	-20	20 21 22 23
7	bisbee	-0.07	0	20	-20	22 32 33 35 36 37 38 39 24 23
8	paleozoic	0.03	0	20	-20	12 16 17 25 26 27 30 31
9	paleozoic	0.04	0	20	-20	24 39 38 37 36 40 41 42 43 44 45 46 26 25
10	bolsa	0.02	0	20	-20	92 30 27 28 29
11	precam-brian	-0.012	1.45E-03	20	-20	29 28 27 26 46 45 44 43 42 41 54 71 77 78 86
12	pantano	-0.45	0	20	-20	34 47 48 49 35
13	bisbee	0.042	0	20	-20	35 49 48 40 36
14	paleozoic	-0.018	0	1	-4	47 50 51 52 53 54 41 40 48
15	paleozoic	0.077	0	20	-20	52 55 56 53
16	alluvium	-0.515	0	20	-20	51 57 58 59 60 61 62 63
17	pantano	-0.313	0	20	-20	51 63 64 65 66 55 52
18	bisbee	-0.012	0	20	-20	55 68 69 70 71 54 53 56
19	paleozoic	0.056	0	20	-20	68 67 74 76 77 71 70 69
20	paleozoic	0.007	0	20	-20	62 72 73 74 67 64 63
21	precam-brian	-0.086	7.00E-04	20	-20	73 75 76 74
22	bisbee	-0.07	0	20	-20	81 1 84 91 85 79 80
23	precam-brian	-0.069	7.00E-04	20	-20	72 82 83 75 73
24	empire stock	-0.022	3.10E-03	20	-20	4 7 31 30 92 89
25	paleozoic	0.044	0	20	-20	89 92 29 86 87 88 5
26	paleozoic	0.04	0	20	-20	84 88 87 90 91
27	precam-brian	-0.02	2.00E-03	20	-20	87 86 78 79 85 91 90
28	paleo onaxis	0.05	0	20	-20	65 64 67 68
29	bisbee onaxis	0.02	0	20	-20	55 66 65 68
30	qtg offaxis	-0.5	0	0	-5	33 34 35